Hydrogeology of the shallow aquifer at the Svelvik ridge

Hydrogeology of the late Pleistocene unconfined aquifer at the Svelvik ridge, Drammensfjorden in southeastern Norway.

Tor Melø

Master Thesis in Geosciences

Discipline: Enviromental Geology and Natural Hazards

Department of Geosciences

Faculty of Mathematics and Natural Sciences

UNIVERSITY OF OSLO

June 1st 2011

© Tor Melø, 2011

Tutor: Per Aagaard, Professor at the Inst. of Geosciences. University of Oslo.

This work is published digitally through DUO – Digitale Utgivelser ved UiO

http://www.duo.uio.no

It is also catalogued in BIBSYS (http://www.bibsys.no/english)

All rights reserved. No part of this publication may be reproduced or transmitted, in any form or by any means, without permission.

Abstract

The Svelvik ridge was approved by local authorities as a CO_2 field lab in 2008 and the appraisal phase for this project was completed in the summer of 2010. This operation gave a valuable insight of the subsurface and provided a good basis for a hydrogeological study of the ridge.

For mapping the vertical extent of the shallow aquifer the electrical resistivity tomography method was used. The models created from these surveys indicated an interface from higher restivity values to lower values located 13 to 20 meters below the surface. These models were compared to flush samples from a drilling operation done in 1981.

The grain size distribution curves from the flush samples were analyzed witht he Hazen and the Gustafson method. The results indicated at the 21 and 24.5 meters the hydraulic conductivity values were in the range of 10^{-7} to 10^{-9} and in the upper 5-7 meters the values were 10^{-4} ms^{-1}.

Based on the comparison the saturated thickness of the aquifer was estimated at 20 meters.

Two methods were applied to obtain estimates of transmissivity and storativity; The tidal forcing method and a conventional pumping test. For the tidal method pressure transducer data loggers were placed in the ocean and in an inland well. The data was analyzed with the Fast Fourier transform algorithm and the results indicated two main cosinouids. These were used to find the phase lag and the amplitude loss in the inland well. The results were used to find the aquifer's diffusivity, which is the ratio between the transmissvitity and storativity. When the aquifer thickness is known, the hydraulic conductivity can be found from the diffuvitiy.

The pumping test were conducted by the Norwegian Geotechnical Institute; the data was fitted to with the Theis analytical solution.

The pumping test gave storage coefficient values from 0.16 to 0.2 depending on the anisotropy ratio and the transmissivities in the order of 10^{-2} m^2s^{-1}. The tidal forcing method resulted in transmissivites in the 10^{-2} to 10^{-3} m^2s^{-1} range.

Preface

The Svelvik ridge is an ice contact system formed during the Ski stage of the Holocene ice recession. It is located in the Drammensfjord in Southeastern Norway. It functions as a natural barrier between the inner and outer fjord basin. The deposit hinders water circulation from the south side and makes the inner fjord basin naturally anoxic.

The site was selected for a field lab for monitoring of subsurface CO_2 behavior; the project is managed by SINTEF Petroleum Research. The decision to use the Svelvik ridge for this project instigated several geophysical measurements as seismic surveys, electrical resistivity tomography (ERT) and ground penetrating radar surveys.

A 300 meter deep well was drilled in the summer 2010 for future gas injection tests. Several shallow wells were also installed during this period. This drilling operation provided a good opportunity to learn field hydrogeology and gain more knowledge about the groundwater behavior at the ridge. This is the main motivation behind this thesis.

Since the factors that govern groundwater behavior and gas behavior are to a large extent similar, the results from this study may be useful in both areas.

Contents

List of figures and tables

List of mathematical symbols

A_r	Anisotropy ratio [unitless]
n_T	Total porosity [%]
h	head [L]
S	Storativity or Coefficient of Storage [unitless]
S_S	Specific storage [m^{-1}]
Sy	Specific yield [unitless]
K	Hydraulic conductivity [LT^{-1}]
b	Aquifer thickness [L]
T	Transmissivity [L^2T^{-1}]
T/S	Aquifer Diffusivity [L^2T^{-1}]
ρ_a	Apparent resistivity [ohmm]
K	Geometric factor [L] (The same symbol is used in ERT and for Hydraulic conductivity values.
V_{MN}	Voltage potential between MN electrodes [Volt]
I_{AB}	Current injected AB electrodes [Amperes]
TE	Tidal efficiency [unitless ratio]
Lag_k	Tidal lag [radians]
P_k	Period of tidal constituent [T]
f_{Nq}	Nyquist frequency [Hz]
Φ(k)	Fourier coefficient [complex]
Φ(k)Z	magnitude of Fourier coefficient [amplitude]
Φ(k)θ	phase of Fourier coefficient [radians]
s	Drawdown in well [L]
M_{sf}	Unisolar synodic fortnightly tidal constituent
M_2	semidiurnal lunar tidal constituent

1 INTRODUCTION

1.1 Research objectives

This thesis aims to characterize the hydrogeology of the unconfined aquifer at the Svelvik ridge. The geophysical method electrical resistivity tomography has been used to give an indication of the vertical extent of the shallow aquifer as well as give an impression of the heterogeneity of the upper layers. The results from these surveys will be compared with samples obtained from previously done drilling operations at the site.

Based on this information of this will give a relative good insight of the subsurface and provide a description of the vertical extent of the shallow aquifer.

For the hydrogeological investigation, three major parameters that govern groundwater behavior will be estimated; they are transmisivity (T), storativity(S) and hydraulic conductivity (K). Two methods will be applied to estimate these parameters; the tidal forcing method as proposed by Ferris (1951) and Todd (1980) and conventional pumping tests aided by the use of analytical models for solutions.

The tidal forcing approach is based on the different characteristics of tide level and the head fluctuations caused by the tidal in an inland observation well. Based on the differences between the two signals it is possible to give rough estimates of the aquifers diffusivity which is the ratio of transmissivity to the storativity.

A pumping test was performed by the Norwegian Geotechnical Institute (NGI) late summer 2010 and the data from has been made available for this thesis. The Theis (1935) analytical solution will be fitted to the pumping test results. This should give good estimates of the transmissivity and the storativity values.

Hydraulic conductivity values for each flush sample will be estimated with the empirical formulas Gustafson (1984) and Hazen (1893).

2 BACKGROUND

2.1 Geological setting

2.1.1 General geology at the site

The deposit is located in Hurum municipality and forms a sill in the Drammensfjord in the south eastern part of Norway. It is a glaciofluvial / marine terminal deposited as the glacier halted in a deglaciation as a response to a period of warming after the *Younger Dryas* cool period (Sørensen 1981). Figure 2.1.1 illustrates the different stages in the Holocene deglaciation. The different stages represent areas where the ice either halted its retreat or readvanced.

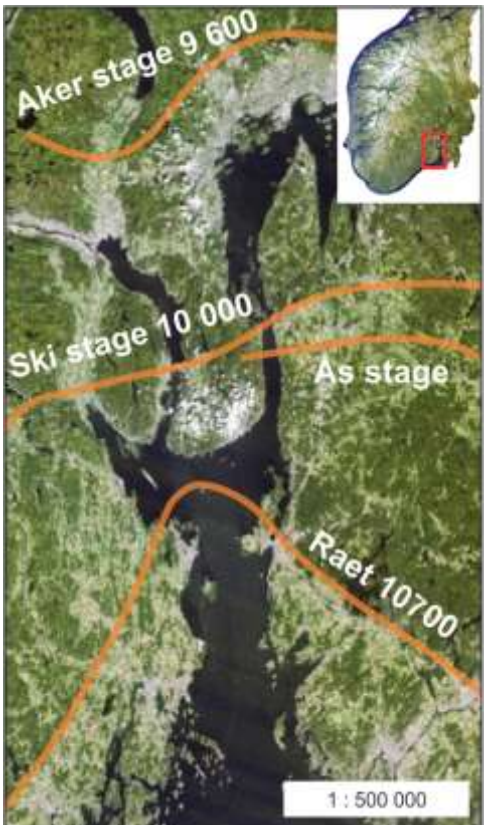

Figure 2.1.1 Holocene Ice recession stages (Modified from Sørensen 1981)

The Svelvik ridge was deposited during the Ski stage approximately 10 000 years ago when the glacier readvanced and it kept its position for a significant time (Sørensen 1981). Smaller scattered moraines in the area suggest that the glacier's front oscillated and was not stationary (Sørensen 1981). At one point the glacier came in contact with the ocean; and subsequently the deposit can be characterized as a glaciomarine ice-contact system.

2.1.2 Ice contact classification

Lønne (1993) proposed a system of classifying ice contact glaciomarine systems. The depositional settings for these kinds of systems are very complex (Lønne 1993). However, in ice contact systems like these the main sedimentary supply comes from two sources; unsorted sub glacial diamictic material and outwash material from the meltwater outflow (Lønne 1993). The sediments of the deposit should then be diamictic in nature as well as showing a varied lithologic composition.

The depositional systems of glaciomarine termini can be classified in three main facies: Ice-contact submarine fans which are totally subaqueous systems; Ice-contact deltas which may

have a small sub aerial component; and lastly glaciofluvial deltas which often have a well-developed sub aerial component (Lønne 1993).

The Svelvik ridge is an ice-contact submarine fan. This is a submarine wedge of coarse grained material which has been deposited subaqueous at the glacier's front edge. The wedge does not have a top set due to lack of stream activity, but it has bedded fore- and bottomset deposits. The sediment was deposited along the major ice front, and effectively shaped the front to that of the glacier (Lønne 1993). The front of a tide water glacier tend to be rather unstable, and is often attributed to calving or oscillatory movements due to the glacier's reaction to climatic changes (Lønne 1993).

The submarine fan was formed by resedimentation of the diamictic glacial material along with ice rafted debris from melting sea ice (Lønne 1993). Figure 2.1.2 illustrates the common features of these kinds of deposits.

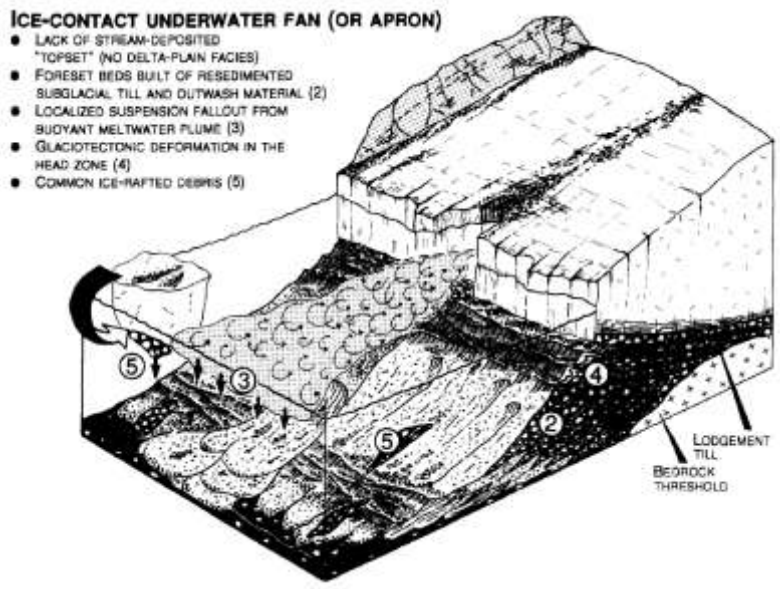

Figure 2.1.2 Model of an Ice-contact submarine fan (Lønne 1993)

By adopting Lønne's idealized model for an Ice-contact submarine fan, these deposits will generally consist of four major sedimentary facies, A, B, D and E (fig 2.1.3)

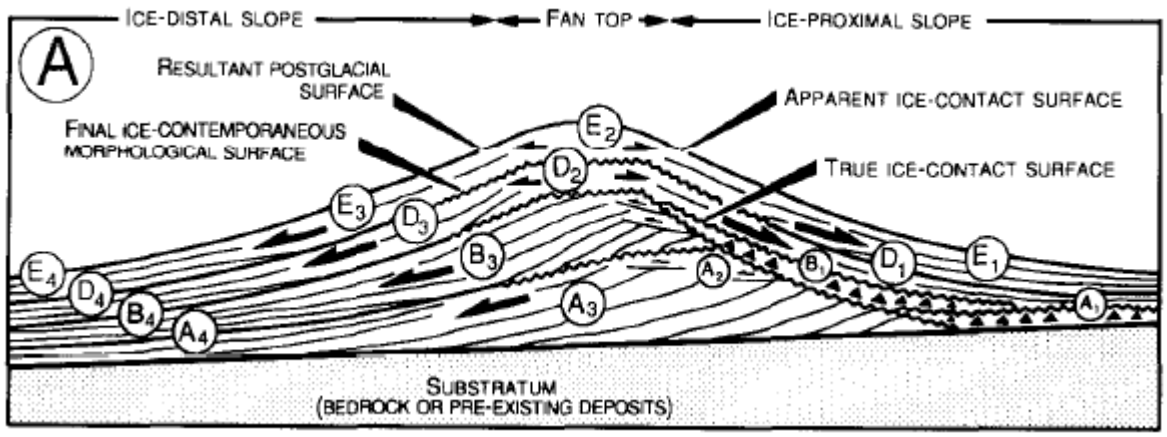

Figure 2.1.3 Idealized model for Ice-Contact fans (Lønne 1993)

Where unit A is the ice-contact facies formed during the glacier's advance. These facies will normally comprise of coarse grained clinoformal foreset deposits (A_3), these will downlap into horizontal bottomset facies consisting with silty mud along with turbiditic sands (A_4) (Lønne 1993). Along with deposition of A_3 and A_4 the ice proximal slope will be subjected to primarily sub-glacial processes such as deposition of basal till and other sorted debris. Deformation is mainly done by the meltwater outflow but if the glacier advances, heavy erosion and further deformation can occur. These A-units may consist of boulder rich foreset beds, basal till with cohesive debris flows (Lønne 1993). The A_2 subunit may be present if the glacier advances across the fan top, and can leave a sub horizontal layer (Lønne 1993).

The B-unit is ice-contact facies formed during a glacier still stand or retreat. These facies may be similar to that of the A-units. The sediment will be coarse grained and may have a high content of subglacially derived debris and ice rafted debris (Lønne 1993).

The D-unit is deposited during the retreat of the glacier terminus, mainly deposited from the hyperpycnal meltwater plume. These will consist of very fine sand and the finer fractions and debris flow deposits. These units tend to drape the front and back slope (Lønne 1993).

The E unit is facies formed during fan uplift. When the glacier retreats the post glacial isostatic uplift may occur. This will have various effects on the deposit by reworking and resedimentation of the original sediments, when the deposit hits the storm wave base and subsequently the fair weather base. This may result in shoreline facies on the proximal and distal sides of the deposit (Lønne 1993). The glacier may also re-advance and repeat the

depositional processes above and further complicate the sedimentary structure of the deposit (Lønne 1993).

For the glacier to halt, a topographical feature like a preexisting moraine or a bedrock threshold should be present. In the Svelvik case the main bedrock threshold is located farther south, as can be observed in figure 2.1.4. There is evidence of a preexisting moraine under the post glacial clay as indicated by the green area under the main deposit in figure 2.1.4 (Bjerkli and Olsen 1984). This can have served as threshold for the glaciers advancement, and it may stem from another glaciation event or from the oscillating glacier's front since there is evidence of smaller scattered moraines in the area (Sørensen 1981).

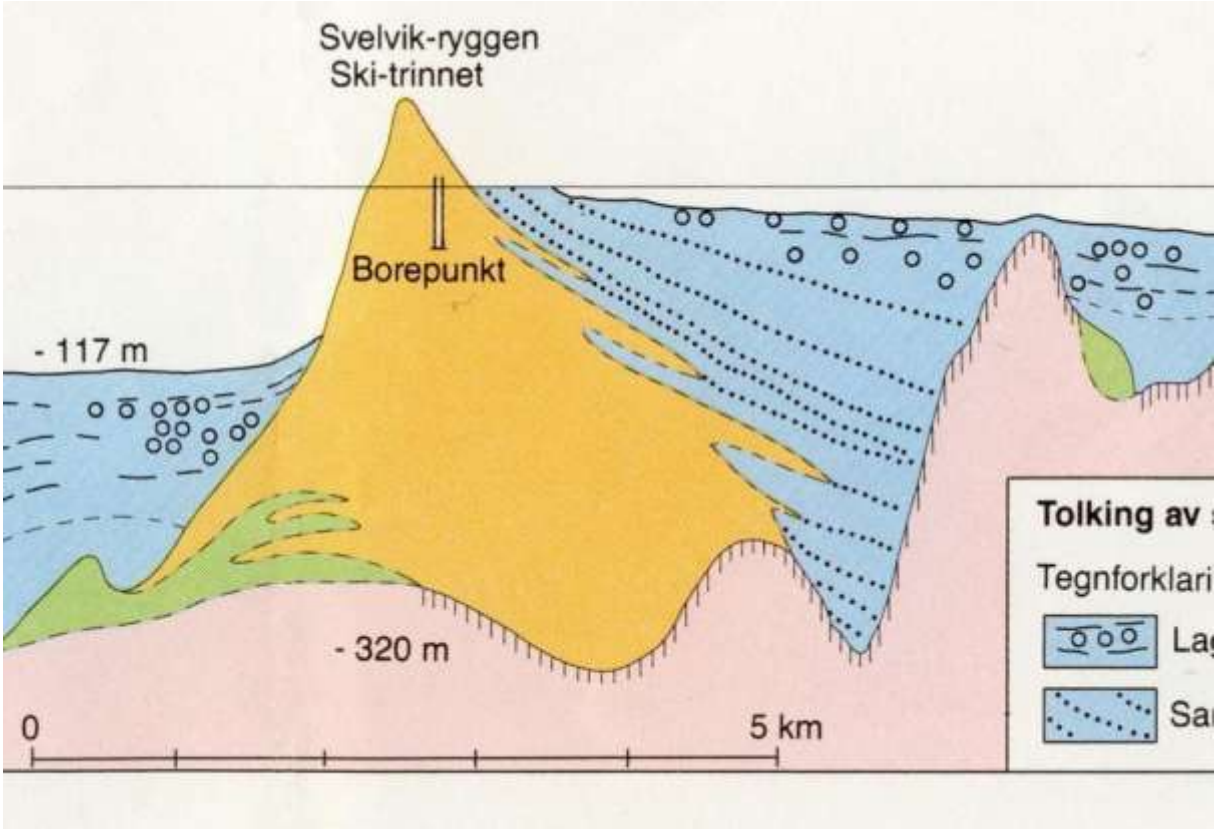

Figure 2.1.4 longitudinal north / south profile (Sørensen et. al 1990)

2.1.3 Post-glacial evolution

After the deglaciation, the original deposit was aerially exposed approximately 7 000 years ago (Sørensen 1981) due to isostatic rebound. The ridge was then exposed to erosional forces as rivers (Sørensen 1981) and in like similar deposits wave and tidal action may have reworked some of the sediments as the deposit reached the storm- and fair weather wave

bases (Lønne 1993). The highest evidence of wave action has been found up to 197 meters above sea level denoting the marine limit in the area (Sørensen 1981).

The tidal current has later cut the upper parts of the deposit, separating the Western and Eastern parts, and is influenced by the semi-diurnal Svelvikstraumen tidal current.

2.1.4 Sediment distribution and bedrock geology

The Quaternary map from Sørensen *et al.* (1990) (figure 2.1.5) illustrates two major sedimentary facies; the marine shore deposits (blue areas) in the southern part and the main glaciofluvial deposit (yellow areas).

Marine shore deposits are sorted, washed and reworked by waves and currents in the shoreface. These often consist of sand and gravel (Sørensen et. al 1990). The surface area of the glaciofluvial deposit is approximately 1.78 km^2 and the surface area of the marine shore deposits is approximately 0.3 km^2 (Sørensen *et al*. 1990).

The coarser grained Drammensgranite dominates the bedrock distribution in the area (Sørensen 1981). This variant of the granite usually has between 3-5 mm grains, less than 3-5 % oligoclase, 30-35 % quartz and between 60-65 % perthitic feldspar (NGU 2011).

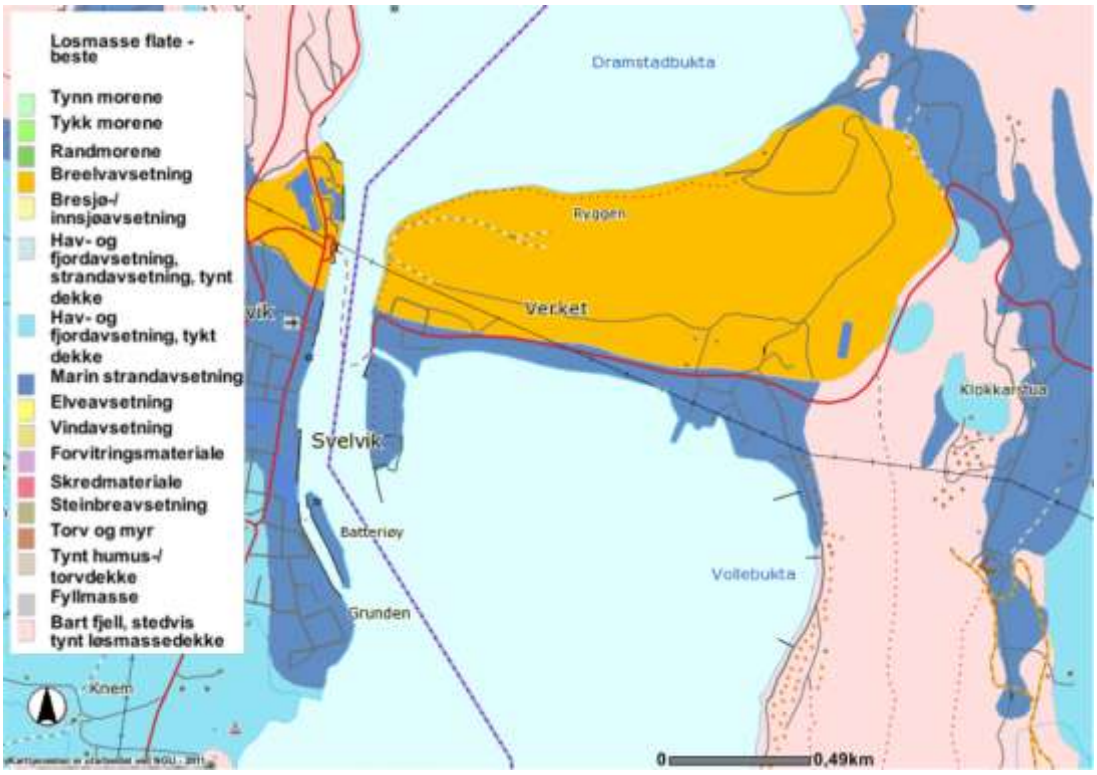

Figure 2.1.5 Quaternary map (Sørensen *et al*. 1990)

2.1.5 Hydrogeology at the site

The Svelvik ridge is thought to consist of two types of aquifers. One of the aquifers is the upper one, with the groundwater table marking the upper limit. The lower limit of this aquifer will be found in this thesis and below this confining layer there may be a confined aquifer. This thesis will focus on the shallow or unconfined aquifer at the Svelvik ridge. In order to do so, the reader will have to be acquainted with the basic hydrogeological concepts, which is introduced and discussed in the next section.

2.2 Hydrogeological concepts

2.2.1 Aquifer concepts and properties

An Aquifer has been described by Driscoll (1986) as a formation, a group of formations, or a part of a formation that contains sufficient saturated permeable material to yield economic quantities of water to wells. There are several types of aquifer types found in nature. The units that separate the aquifers from other geological formations are called confining beds. These are units of low permeability which limits or hinders the flow of water. They may be referred to as aquiclude or aquitard depending on the nature of how permeable they are. The aquifuge is not permeable at all, and the aquitard is to a degree permeable, but not in a large extent (Schwartz and Zhang 2003).

Unconfined aquifers are defined by the water table forms the upper boundary. Any wells in this type of aquifer will approximately indicate the position of the water table. Confined or artesian aquifers are confined with low permeable layers around them. Wells which penetrates the aquifer will reveal that the water table lies above the upper boundary (Schwartz and Zhang 2003). There is also a leaky aquifer type, which is an aquifer bonded by aquitards. This will produce a slight artesian pressure in the aquifer resulting in that the water table can be found slightly above the upper confining layer (Krusemann and de Ridder 1992).

These descriptions are end members, and in nature it occurs often a mixture of all three in one formation. An aquifer system can be very complex so simplifications have to be made by assumptions.

2.2.2 Anisotropy

For many groundwater investigations it is assumed that the aquifer has the same properties in all directions. This is homogeneity (Driscoll 1986), and can in many cases be far from the true nature of the aquifer. The concept of isotropy is also often used in groundwater investigations; this implies that the properties of the medium are the same in all directions (Driscoll 1986). This might also not be the case as the individual particles tend to settle on their flat sides, if they are not completely rounded. This will influence the direction which has the higher permeability and often the horizontal direction will dominate (Krusemann and de Ridder 1992).

The anisotropy ratio (A_r) is introduced to give an estimate of the layering of the aquifer. It can be described as:

$$A_r = \frac{K_h}{K_v} \qquad (2.2.1)$$

In equation 2.2.1 the K_h is the horizontal hydraulic conductivity [LT^{-1}] and the K_v is the vertical hydraulic conductivity [LT^{-1}]. The ratio between these is the anisotropy ratio and is unitless.

2.2.3 Porosity

The total porosity (n_T) of a medium can be described as the ratio of the void volume to that of the total volume of the rock (Schwartz and Zhang 2003). Mathematically it can be described as in equation 2.2.2:

$$n_T = \frac{V_v}{V_T} = \frac{V_T - V_S}{V_T} \qquad (2.2.2)$$

However, not all pores in a medium may be connected to each other, thus lowering the flow between them. The parameter effective porosity (n_e) is introduced to account for this. However, the porosity indicates how much water an aquifer can hold, but not how much it will yield (Driscoll 1986).

How much water a representative volume from an aquifer will release by the force of gravity is called the specific yield (S_y). How much is retained is denoted as the specific retention. The sum of these two factors equals the porosity. The ratio between these depends largely on the grain size, and smaller grain sizes have higher retention resulting from higher surface tension than coarser sediments and usually range between 0.01 and 0.3 (Driscoll 1986).

2.2.4 Storativity or the coefficient of storage

One of the criteria for a geological formation to be an aquifer is that is has to have the ability to store water. The way the aquifer stores water depends on whether the aquifer is confined or unconfined. For the unconfined aquifer the main source of water is the decline in the water table as a response to pumping (Schwartz and Zhang 2003). The storativity can then be defined as the volume of water an aquifer releases or takes into storage per unit surface area of the aquifer per unit change in head (Schwartz and Zhang 2003). It can be described as:

$$S = \frac{Volume\ of\ water\ [m^3]}{(Area[m^2])(Head\ change[m])} \qquad (2.2.3)$$

Equation 2.2.3 illustrates that S, the storativity is a dimensionless number. For a related term to the storativity, the specific storage (S_s) can be described as (Schwartz and Zhang 2003):

$$S_s = \frac{Volume\ of\ water\ [m^3]}{(Area\ [m^2])(b\ [m])(Head\ change\ [m])} \qquad (2.2.4)$$

In equation 2.2.4, b is the aquifer thickness. The specific storage has a dimension of [m^{-1}]. For storage in unconfined aquifers the relation is expressed as equation 2.2.5 (Schwartz and Zhang 2003):

$$S = S_s b + S_y \quad (2.2.5)$$

Krusemann and de Ridder (1992) estimated for sand and gravel the value for S_s are in the order of 10^{-3} m^{-1}. This makes the first term close to negligible, resulting in for unconfined aquifer the storativity is dominated by the specific yield (Schwartz and Zhang 2003).

2.2.5 Hydraulic conductivity and transmissivity

Darcy's law can be used to explain the concept of hydraulic conductivity. For laminar flow conditions it can be stated as (Schwartz and Zhang 2003):

$$\frac{Q}{A} = K - \frac{dh}{dl} \qquad (2.2.6)$$

Equation 2.2.6 is known as the Darcy's equation, where K [LT^{-1}] is the hydraulic conductivity, $\frac{dh}{dl}$ is the hydraulic gradient [unitless], Q [m^3] is the discharge and A [m^2] is the cross sectional area of a tube which water flows through. The hydraulic head is the energy available for groundwater flow. However, under normal circumstances the head is calculated as a column of water over a certain datum (Driscoll 1986). For this survey, the head is calculated as the water level above the NN1954 datum.

Table 2.2.1 gives representative values of hydraulic conductivity for various types of unconsolidated sediments.

Table 2.2.1 Values for hydraulic conductivity for some types of unconsolidated materials

Material	**Hydraulic Conductivity (m/s)**
Gravel	$3x10^{-4}$ to $3x10^{-2}$
Coarse sand	9×10^{-7} to 6×10^{-3}
Medium sand	9×10^{-7} to 5×10^{-5}
Fine sand	2×10^{-7} to 2×10^{-4}
Silt	1×10^{-9} to 2×10^{-5}
Clay	1×10^{-11} to 4.7×10^{-9}
Unweathered marine clay	8×10^{-13} to 2×10^{-9}

(Source: Domenico and Schwartz 1998)

Transmissivity is closely related to the hydraulic conductivity. It can be described as the ease of flow of water through an aquifer (Driscoll 1986). It is the product of the hydraulic conductivity (K) and the thickness of the aquifer (b). Mathematically it is stated in equation 2.2.7:

$$T = Kb \qquad (2.2.7)$$

It has the units of $[L^2T^{-1}]$.

2.2.6 Groundwater flow equations

In an unconfined aquifer the principal equation that governs groundwater flow in an unconfined aquifer is expressed as (For a complete derivation of this equation see Schwarz and Zhang 2003):

$$\frac{\partial}{\partial x}\left(K_x \frac{\partial h}{\partial x}\right) + \frac{\partial}{\partial y}\left(K_y \frac{\partial h}{\partial y}\right) + \frac{\partial}{\partial z}\left(K_z \frac{\partial h}{\partial z}\right) = S_s \frac{\partial h}{\partial t} \qquad (2.2.8)$$

In equation 2.2.8 the x, y and z denotes the flow directions. K is the hydraulic conductivity, h is the head and t is time.

Often in hydrogeological investigations an isotropic aquifer is assumed. Isotropy can be expressed mathematically as ($K_x = K_y = K_z$). The hydraulic conductivity is the same in all directions. Aquifers are also often assumed to be homogeneous, this can be expressed as $K_{x,y,z}$ = constant.

Equation 2.2.8 can be expressed in many ways depending on the flow conditions. Assuming one dimensional flow in the x direction, and isotropic and homogeneous aquifer; and by multiplying with the aquifer thickness (b) and dividing with the transmissivity (T) on both sides the equation in 2.2.8 simplifies to:

$$\frac{\partial^2 h}{\partial x^2} = \frac{S \partial h}{T \partial t} \qquad (2.2.9)$$

Where in equation 2.2.9, h is the head, S is the storativity, T is the transmissivity of the aquifer and t is the time. The ratio between the transmissivity and storativity is denoted as the aquifer's diffusivity.

The tidal forcing method presented in section 3.3.3 estimates the aquifer diffusivity based on equation 2.2.9, and by using known values for the storage coefficient it is possible to find transmissivity values, and subsequently hydraulic conductivity values for the aquifer.

2.2.7 Empirical Hydraulic conductivity formulas

There have been many attempts to link the distribution of the different grain sizes to that of the hydraulic conductivity. Two empirical formulas will be described here to give estimates of the vertical distribution of this parameter.

Hazen (1893) proposed a method of estimating the hydraulic conductivity through grain size analysis. An empirical formula for the relation between the effective diameter (d_{10}) and the hydraulic conductivity is expressed mathematically in equation 2.2.10 (Gustafson *et al*. 1984):

$$K = 0.01157\ d_{10}^2 \qquad 2.2.10$$

A prerequisite for successful use of this formula is that the ratio of $d60 / d10 \leq 5$, this is also known as the uniformity coefficient (Gustafson *et a.l* 1984).

Gustafson *et al.* (1984) proposed another method of estimating the hydraulic conductivity based on the d_{10} and d_{60} distributions. This function is presented in equation 2.2.11.

$$K_{50} = E(U)D_{10}^2 \qquad (2.2.11)$$

Where

$$U = \frac{D^{60}}{D^{10}} \qquad \text{(I)}$$

$$E(U) = 10.2E^6 \frac{e^3}{1+e} \frac{1}{g^2(U)} \qquad \text{(II)}$$

$$e = 0.8\left(\frac{1}{2\ln(U)} - \frac{1}{U^2-1}\right) \qquad \text{(III)}$$

$$g(U) = \frac{1.3}{\log(U)} \frac{U^2-1}{U^{1.38}} \qquad \text{(IV)}$$

With the aid of these formulas the hydraulic conductivities will be estimated in section 4.1.1

2.3 Electrical resistivity method

2.3.1 Theory and application of the electrical resistivity method.

The 2D resistivity method is a geophysical method which gives insight in the subsurface lithology without any serious invasion of the subsurface. This method aims to establish the electrical properties of the subsurface by making measurements on the surface. Based on the electrical properties it is possible to evaluate the subsurface conditions geologically.

Most geological materials conduct electricity; however some have higher resistivity values than others. For unconsolidated sediments the subsurface resistivity depends largely on five main parameters (Bernard 2003).

- In the water saturated zone the current are carried by ions. This is called electrolytic conductibility (Bernard 2003). This makes the presence of water, which often coincides with porosity in the water saturated zone, a major parameter determining the electrical conductivity of the subsurface.
- Another important parameter is how well the pore fluid carries the current. This is governed by the amount of dissolved solids in the pore fluid. This is an important factor to when measuring the electric resistivity of the subsurface.
- Owing to a good ion exchange properties, most clays conduct electricity well (Bernard 2003).
- Any presence of metallic minerals as well as graphite or pyrite will decrease the resistivity of rocks. This is electronic conductibility, where the current is carried by displacement of electrons (Reynolds 1997).
- Lastly, any change in temperature will also have an implication for the electrical conductivity (Reynolds 1997).

It is important to emphasize that the results are equivocal, since the electrical resistivity values for different materials overlap, as shown in figure 2.3.1. The results should not be interpreted categorically, but be used as a guide, keeping the depositional environment and other geological conditions in mind when interpreting resistivity data.

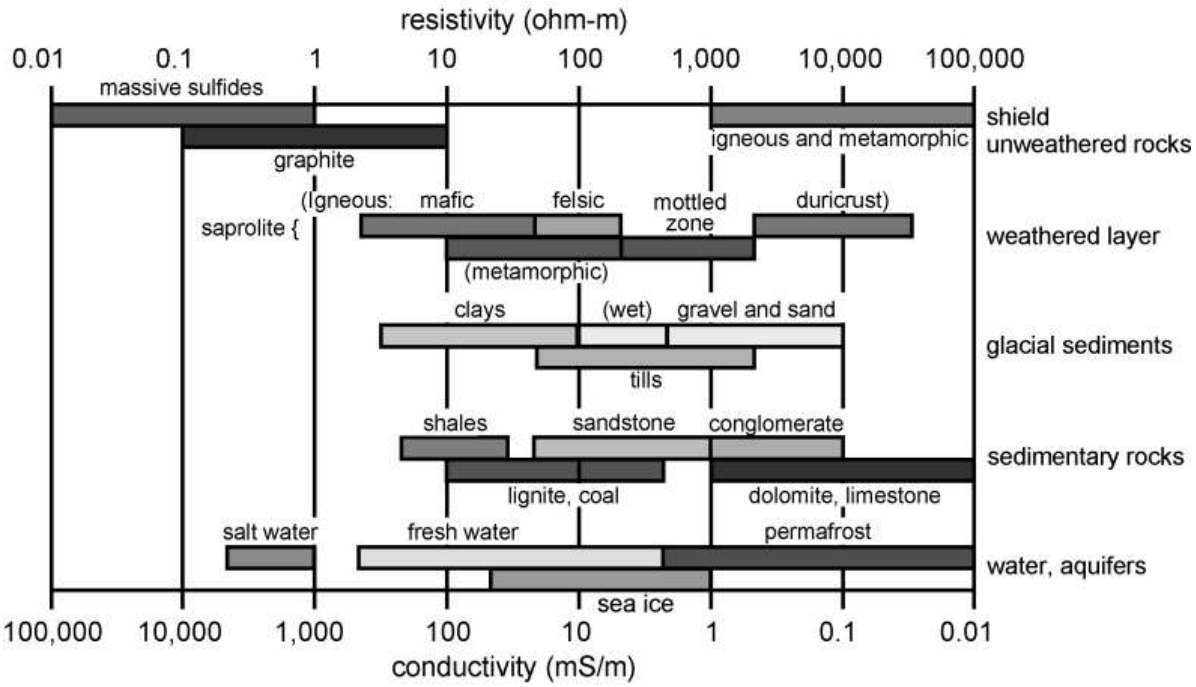

Figure 2.3.1 Values for geological materials (Palacky 1987)

2.3.2 Measuring principles

The surveys are carried out by injecting a direct electrical current (I) [A], in the ground using two current electrodes (A and B). The potential voltage difference (ΔV) [V], and is then measured by two additional electrodes (M and N). Figure 2.3.2 shows this setup.

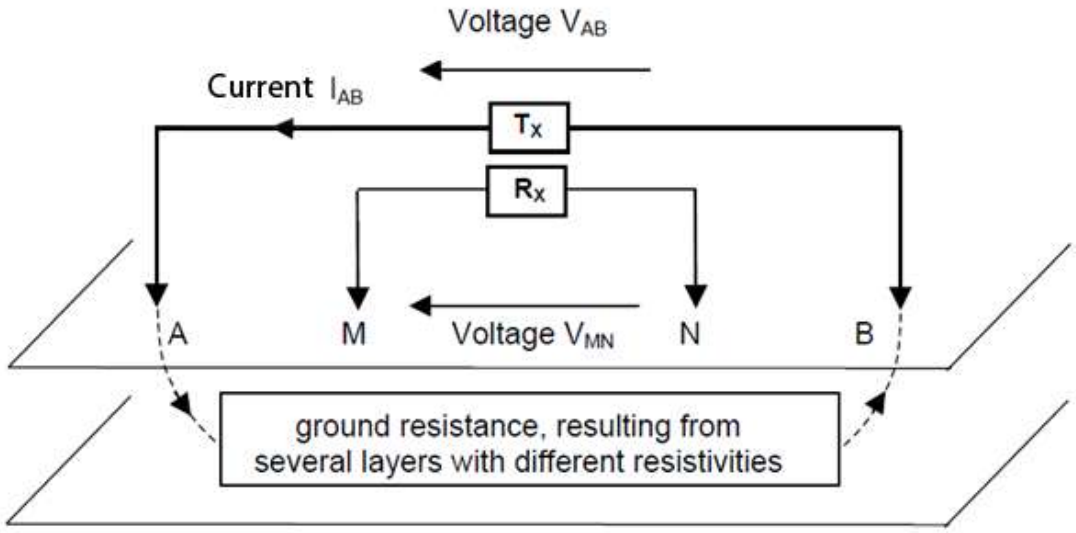

Figure 2.3.2 Resistivity survey setup (Bernard 2003)

The transmission circuit,$I_{AB} = \frac{V_{AB}}{R_{AB}}$ where *I* [A], *V* [V], and *R* is the resistance between the ground electrodes [ohm].

The apparent resistivity (ρ_a) is then calculated from measurement in the receiver circuit. The ΔV is the voltage potential between the MN electrodes. This relation can be expressed as (Reynolds 1997):

$$\rho_a = \frac{\Delta V}{I} K \qquad (2.3.1)$$

Where in equation 2.3.1, K is the geometric factor [L]; the value is dependent on the electrode configuration.

For a homogeneous medium the apparent resistivity [ohmm],ρ_a will be the same as the true or specific resistivity. However, encountering homogeneous media in nature are rarely the case. For a heterogeneous subsurface the distribution of ground resistivity must be modeled with appropriate computer software.

The depth of the investigation is to a large extent dependent on the total length between the two current electrodes and on the separation between the potential electrodes (Bernard 2003). The total investigatory depth (*d*) for a dipole-dipole survey can be estimated by using d = 0.17L (Barker 1989), where *L* is the distance between the two current electrodes.

A more practical limitation is the measurability of the V_{MN} (Bernard 2003), which can be expressed as in equation 2.3.2:

$$V_{MN} = \frac{\rho I_{AB}}{K} \qquad (2.3.2)$$

This shows that the measured voltage potential is dependent on the ground resistivity. A higher ground value, e.g. gneiss which is in the range of 10^3 ohmm (Reynolds 1997) will produce a stronger signal than e.g. unconsolidated sand which often lies in the 100s ohmm (Reynolds 1997). The geometric factor, *K*, is also very important factor, especially for large investigation depths, which again will result in the V_{MN} to become very small and consequently immeasurable, or largely dependent on the instruments ability to record very low voltages.

For measurements in glaciofluvium, the top unsaturated layer often has a low conductivity, thus the current (I_{AB}) in the transmission circuit can become low. In most cases the ground

conductivity is a non-changeable parameter, but in unconsolidated soils it might be changed by adding an electrolyte fluid around the electrodes to ensure lower resistivity.

There are many different electrode configurations, as Wenner and Schlumberger. The Schlumberger array is often applied to find vertical changes of the electrical properties, and is often called Vertical electrical sounding (VES) (Reynolds 1997). The Wenner array is used to map lateral variations of the electrical properties, and is called Constant separation traversing (CST) (Reynolds 1997).

However a method which uses both of these classical methods to measure both lateral and vertical electrical properties is the Dipole-Dipole array. The array configuration can be illustrated as in figure 2.3.3:

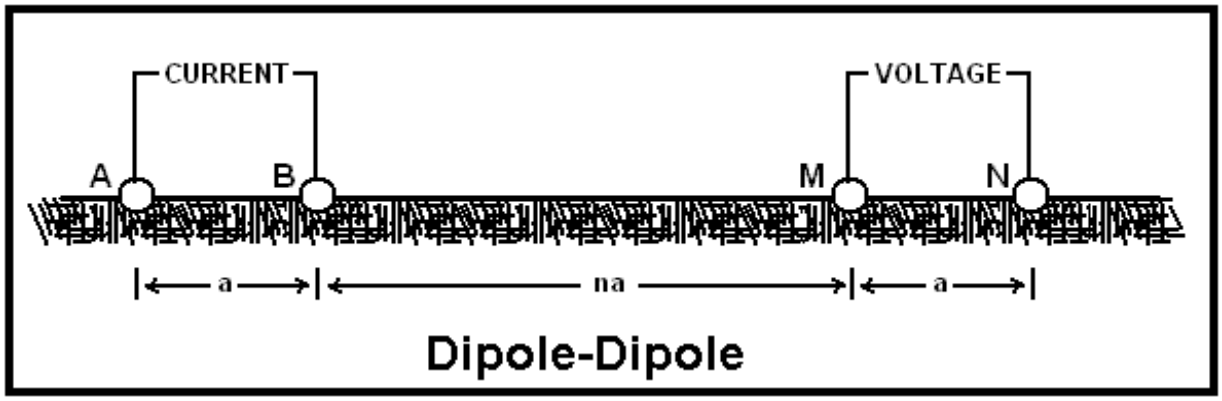

Figure 2.3.3 Dipole-Dipole array (modified from Reynolds 1997)

The MN dipole is moved and measured a fixed times away from the AB dipole. The recorded data is stored as a report point. As the n increases the depth also increases. The AB is shifted one spacing, and the measurements are then repeated (Reynolds 1997). The resulting data is then composed into an *x–z pseudosection* consisting of the report points. This method is sometimes referred to as electrical resistivity tomography.

The geometric factor for the DD array is: $K = \pi n(n+1)(n+2)aR$ (Reynolds 1997). This will often result in higher values than the Wenner array which has a geometric factor of 2πR (Reynolds 1997). This makes the DD array disposed to noisy data sets and will often require more current or longer pulses injected in the subsurface to improve the signal to noise ratio.

2.3.3 Noise and stacking

Noise is a very important factor to take into consideration when performing resistivity measurements. Since the measure voltage potential is in the order of mV, the recording instrument has to be very delicate. This makes it vulnerable to background noise, which may stem from telluric currents; self-potential and industrial noise (Reynolds 1997). Figure 2.3.4 illustrates the effect that this noise has on the V_{MN}. To improve the signal to noise ratio, the concept of stacking is introduced.

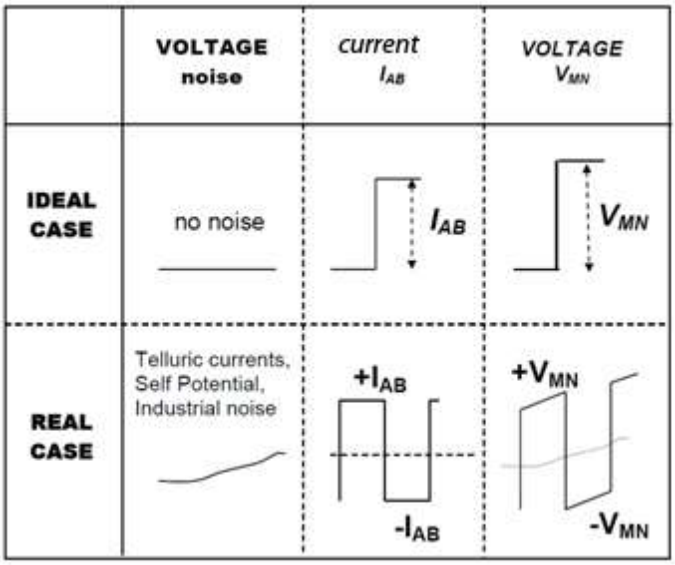

Figure 2.3.4 the influence of noise in resistivity measurements (Bernard 2003)

The stacking procedure is controlled by the Q [%] which is the quality factor. Two measurements from the same report point are compared. If they fall outside the range given by quality factor, the measurements are run until the measurements is within the range or to a maximum number of readings.

2.3.4 2D inversion of the data and inversion parameters

The aim of this step is to create a *x*-*z* model grid model with specific resistivity values. This is done by applying an appropriate inversion algorithm to the the recorded peseudosections (Solberg *et al*. 2011). It is recommended that any bad measurements or very noisy data is removed before reading the file into the inversion program (Hauck and Kneisel 2008). These bad values are often easy to recognize and will be significant dissimilar from the adjacent values in the pseudosection (Hauck and Kneisel 2008).

The depth of an aquifer is often defined by a relative sharp boundary between a less conductive and higher conductive layer (Bernard 2003). When these geological conditions are anticipated the "*robust inversion*" is often used (Kneisel and Hauck 2008). To further accentuate horizontal structures the horizontal / vertical ratio should be set to 0.5 (Solberg *et al*. 2011).

The inversion can be described as (Kneisel and Hauck 2008):

1. A homogeneous earth is used as a starting model is created by calculation of the logarithm of the apparent resistivity values
2. This model is then used to calculate the a set of the apparent resistivities as it would be if this model represented the real values obtained in the field.
3. The difference between these two models are then reduced by an iterative process. The resultant model is then improved on by assigning each measurement to a blocks in the model. This block model is the resistivity model.
4. Lastly, the error between the resistivity (calculated) model and the apparent values (measured), is given by the root mean square error. It should be noted that a low RMS values does not neccecarlily indicate that the model reflect the natrual surroundings better.

2.4 Ferris' Tidal forcing method

2.4.1 General description of the method

Ferris (1951) proposed a method to estimate the hydraulic diffusivity of an aquifer based on the well response from tidal activity. This method has later been elaborated on by several, for this thesis the formulas and theory proposed by Smith and Hick (2001) will be used as a point of departure.

There are several criteria for the use of this method; the first and most obvious is that the aquifer has to adjoin a tidal body (Ferris 1951). Another prerequisite for the method is that the tidal signal must be allowed to transmit through the subcrop, in other words there should be no confining or disturbing structures between the shoreline of the aquifer and the observation location.

The method draws on many similarities to conventional pumping tests, where the groundwater level is measured in observation wells as a response to an external factor. The tidal signal can be viewed as a series of cosines with varying amplitude and wavelength. These cosines are the result of an astronomical body or they may stem from interference from bathymetric or topographical features. Each signal which can be attributed to an astronomical body is called a tidal constituent, and there has been identified more over 400 worldwide. However, the most prominent are the diurnal and semi-diurnal Moon and Sun constituents denoted as M and S, respectively (Defant 1961). Any subscript indicates the periodicity of the constituent.

The main constituents can be obtained through a harmonic analysis and their frequencies should then compared to known constants (Defant 1961), which there are over 400 identified. The signals from each constituent are attenuated differently as it propagates through the aquifer depending on their amplitude and wavelength (Ferris 1951). Two main factors describe the attenuation of the tidal trace; the tidal efficiency (TE) and lag (Ferris 1951).

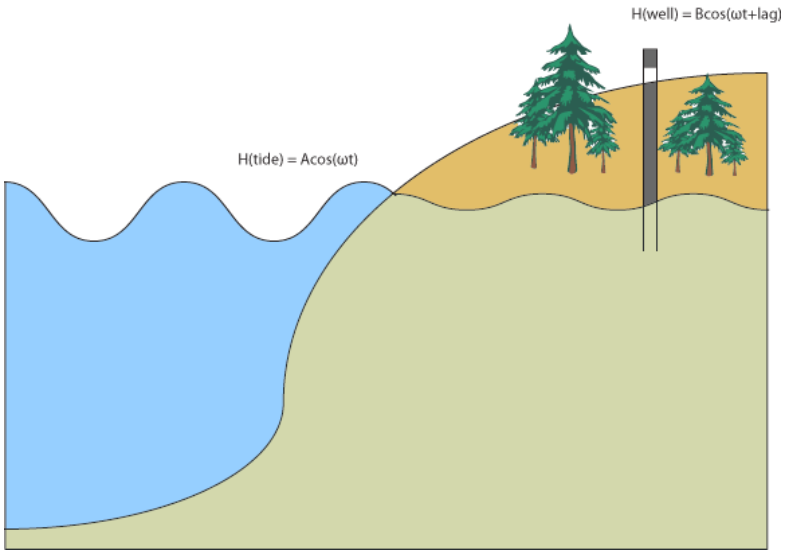

Figure 2.4.1 Concepts of the tidal method

Figure 2.4.1 gives a crude visual representation of the tidal method. The tidal level behaves as a sinusoid. This sinusoidal signal is then transmitted through the permeable subcrop and will be attenuated by two main factors (Ferris 1951); amplitude loss and phase lag. The attenuation of the amplitude is given by the ratio of A and B. The lag is the "+ lag"[rad] in the inland observation well.

2.4.2 Tidal efficiency

The tidal efficiency is the ratio of the amplitude of head fluctuations in a well to the amplitude of the tidal fluctuations. It is described mathematically in equation 2.4.1 (Erskine 1991):

$$TE = \frac{\sigma_{well}}{\sigma_{tide}} \qquad (2.4.1)$$

Where, σ is the standard deviation of the observations. It is a robust method, however another measure is available. This method discriminates between the different tidal constituents. It can be expressed mathematically as (Smith and Hick 2001):

$$TE_k = \frac{well_{ak}}{tide_{ak}} \qquad (2.4.2)$$

In equation 2.4.2 the k denotes the tidal constituent and (a) is the amplitude.

2.4.3 Tidal lag

The lag is dependent on the tidal constituent and can be described as (Smith and Hick 2001):

$$lag_k = well_{\theta k} - tide_{\theta k} \qquad (2.4.3)$$

In equation 2.4.3 (θ) denotes the phase of the constituent (k). This means a slower propagation of the signal will return a longer time lag.

2.4.4 Deriving formulas for aquifer diffusivity based on lag and efficiency.

By using formula 2.2.9 and boundary condition x = 0, (Smith and Hick 2001):

$$h(0,t) = H_a \cos(\omega t - H_\theta) \qquad (2.4.4)$$

Where h is the head, (H_a) is the amplitude of the tidal signal and (H_θ) is the phase [rad].

Formula 2.2.9 and 2.4.4 are linear so they can be broken down into a steady state flow and harmonic flow problem of one or more frequencies. See Smith and Hick (2001) for a more detailed derivation of these formulas.

The harmonic solution can then be rearranged to give expressions for efficiency (equation 2.4.5) and lag (equation 2.4.6) (Smith and Hick 2001):

$$\frac{T}{S} = \frac{\pi x^2}{(\ln TE_k)^2 P_k} \qquad (2.4.5)$$

$$\frac{T}{S} = \frac{x^2 P_k}{4\pi (lag_k)^2} \qquad (2.4.6)$$

Where (x) is the distance from the tidal boundary, S is the storativity. T is the transmissivity, it should be noted that this assumes isotropy, e.g. the transmissivity is uniform throughout the aquifer. The P_k is the period of the tidal constituent. The efficiency based formula (2.4.5) has a logarithmic relationship with the aquifer's diffusivity, whereas the lag based formula (2.4.6) has a linear relationship.

2.4.5 Fourier analysis

To find the dominant frequencies from the aquifer observations a harmonic analysis was done. This was done with Matlab's intrinsic FFT function. This is the discrete Fourier transform algorithm, which produces a discrete frequency domain representation of a sampled signal. The inverse FFT algorithm transforms the frequency domain back to the time domain. The discrete Fourier transform for a data series of *N* length is defined mathematically in equation 2.4.7 (Weisstein 2002):

$$\Phi(k) = \sum_{j=1}^{N} x(j) W_N^{(j-1)(k-1)} \quad (2.4.7)$$

Where Φdenotes the Fourier coefficient and k is is the frequency and W_N is $e^{(2\pi i)/N}$.

The FFT fits N/2 frequencies to N data points. To ensure that all Fourier components of the signal are found, it is necessary to use a sampling rate at least twice the highest frequency. This can be found with the Nyquist condition.

The Nyquist frequency describes the range of the frequency domain. Expressed mathematically it is (equation 2.4.8) (Weisstein 2002):

$$f_{Nq} = \frac{1}{2\Delta t} \quad (2.4.8)$$

Where in equation 2.4.8, Δt is the sampling intervals [s].

The Fourier coefficients are complex so they can be expressed as in equation 2.4.9 (Weisstein 2002):

$$z \equiv x + iy = |z| e^{i\theta} \quad (2.4.9)$$

Where ($|z|$) is the magnitude and θ is the phase of the Fourier coefficient.

The magnitude is given by equation 2.4.10 (Weisstein 2002).

$$|z| = \sqrt{x^2 + iy^2} \quad (2.4.10)$$

These results can be used to find which tidal constituents are dominant using an amplitude spectrum. The amplitude spectrum will result in peaks at the frequencies with high energy. This can be used to isolate the tidal constituents and find the amplitude loss between the two

measuring points. Further by plotting the phases it is possible to find the shift in phase between the two points. The results from this will be presented in section 4.3.

2.5 Aquifer Testing

2.5.1 General theory behind pumping tests

The basic principle behind test pumping is to extract water from a well at a known rate. As the well is pumped, the effect on the water table is measured in the surrounding wells with either manual or automatic logging equipment. The data is then presented graphically and depending on the characteristics of the aquifer an analytical model is fitted to the data. Based on these models the characteristics of the aquifer can be estimated (Krusemann and de Ridder 1992).

2.5.2 Theory of pumping tests in an unconfined aquifer

When pumping an unconfined aquifer results in a different behavior of the water table and thus a different drawdown curve than a confined aquifer. When the cone of depression forms, the saturated aquifer thickness as well as the transmissivity will decrease as illustrated in figure 2.5.2. In addition, the method of releasing water is time dependent (Schwartz and Zhang 2003). There are three main time dependent features of an idealized unconfined aquifer pumping test curve.

At early time the water is released from storage owing to compression of the matrix and expansion of the water. For the drawdown curve this gives the same response as in a confined aquifer, and subsequently the Theis-curve will be similar, and also the storativity values will be similar (Schwartz and Zhang 2003).

At intermediate time the similarities end, owing to the gravity drainage from the matrix as the cone of depression lowers the water table. The drawdown pattern is dependent on the anisotropy concerning the hydraulic conductivity and the saturated thickness of the aquifer (Schwartz and Zhang 2003). The intermediate drawdown is often less than expected, resembling that of in a leaky aquifer (Schwartz and Zhang 2003).

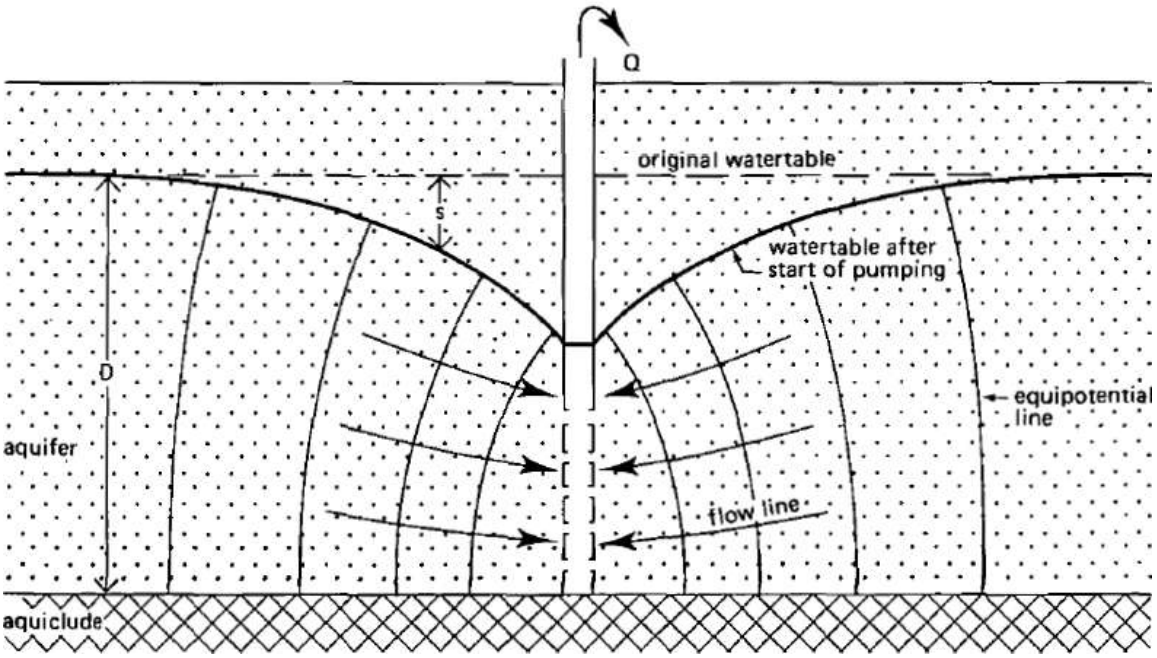

Figure 2.5.2Pumping in an unconfined aquifer principle (Krusemann and de Ridder 1992)

At late time drawdown the effect of delayed gravity drainage subsides and the drawdown curve will again fall on a Theis-curve. The flow is then mainly radial, and the storativity values are now the same as the specific yield (Schwartz and Zhang 2003). These three phases during pumping will result in a sigmoid shaped drawdown curve, as illustrated in figure 2.5.3b.

2.5.3 Theis analytical solution for pumping tests

Numerous models are available for this purpose. Theis (1935) proposed a solution for confined aquifers to estimate the transmissivity and storativity values.

The Theis analytical solution applies to confined aquifers under transient conditions. The flow equation which describes the hydraulic head under these conditions can be expressed mathematically as (Schwartz and Zhang 2003):

$$\frac{\partial^2 h}{\partial r^2} + \frac{1\partial h}{r\partial r} = \frac{S\partial h}{T\partial t} \qquad (2.5.1)$$

In equation 2.5.1, h is the hydraulic head, r is the radial distance from the pumped well to the monitoring well. (t) is the time since the pumping started, and S is storativity and T is transmissivity of the aquifer.

The initial (I) and two boundary conditions apply (II & III), and they are (Schwartz and Zhang 2003):

$$h(r,0) = h_0 \quad \text{(I)}$$

$$h(\infty,t) = h_0 \quad \text{(II)}$$

$$\lim_{r\to\infty}\left(\frac{\partial h}{\partial r}\right) = \frac{Q}{2\pi T} \quad \text{(III)}$$

Where the first condition is for t = 0 and at any distance (r) from the well the head is equal to the initial head (h_0).

The second condition states that at for an infinite radius for infinite time the head is fixed at h_0. This can be seen as one boundary.

The last condition assumes a fixed pumping rate (Q), and is another boundary condition.

The solution to this is attributed to Theis (1935) and can be expressed mathematically as (Schwartz and Zhang 2003):

$$h_0 - h = s = \frac{Q}{4\pi T}W(u) \qquad (2.5.2)$$

Where in equation 2.5.2 the Q is the discharge rate from the pumped well and T is the transmissivity of the aquifer. The s is the observed drawdown [L]. The well function W (u) can be expressed mathematically as (Schwartz and Zhang 2003):

$$W(u) = \int_u^\infty \frac{e^{-y}}{y}dy = -0.577216 - \ln(u) + u - \frac{u^2}{2!2} + \frac{u^3}{3!3} + \frac{u^4}{4!4} + \cdots \qquad (2.5.3)$$

And for the dimensionless variable u is presented in equation 2.5.4:

$$u = \frac{r^2 S}{4Tt} \qquad (2.5.4)$$

The function in 2.5.3 is rather complicated, and it is often evaluated by using well function tables or computer specialty computer applications.

This model was created for the use of confined aquifers, and is generally not transferable for unconfined aquifer analysis.

However, an updated version of the Theis model is available and will take into account the delayed gravity drainage by correcting the drawdown value with (Krusemann and de Ridder 1992):

$$s = b - (b^2 - 2s'b)^{1/2} \qquad (2.5.5)$$

Where in equation 2.5.5, s is the drawdown of the unconfined aquifer, s' is the drawdown for the assumed confined aquifer, as b is the saturated thickness. This correction only applies to the late time drawdown data which theoretically will fall on the Theis curve (Krusemann and de Ridder 1992). Schwartz and Zhang (2003) claims that for larger distances the Theis model for confined aquifers can be fitted to unconfined aquifers without too much error.

2.5.4 Theis assumptions

There are several assumptions for the unconfined Theis solution. They are (Krusemann and de Ridder 1992):

1. Aquifer has infinite areal extent
2. Aquifer is homogeneous, isotropic and of uniform thickness
3. Pumping well is fully or partially penetrating
4. Flow to pumping well is horizontal when pumping well is fully penetrated
5. Aquifer is unconfined
6. Flow is unsteady
7. Water is released instantaneously from storage with decline of hydraulic head
8. Diameter of pumping well is very small so storage in well can be neglected
9. No delayed gravity response in aquifer
10. Flow velocity is proportional to the tangent of the hydraulic gradient instead of the sine.
11. Flow is horizontal and uniform in a vertical section through the axis of the well
12. Displacement is small relative to saturated thickness of aquifer

The data requirements are:

- Pumping and observation wells locations.
- Pumping rates
- Observation well measurements (time and displacement)
- Partial penetration depths
- The saturated thickness of the aquifer
- Hydraulic conductivity anisotropy ratio

2.5.5 Diagnostic plots for determining flow regimes

In well test analysis the diagnostic plots consists of drawdown and its logarithmic derivative versus time. It is most often plotted on log-log scale. These plots play an important role when choosing the analytical model to fit the drawdown data.

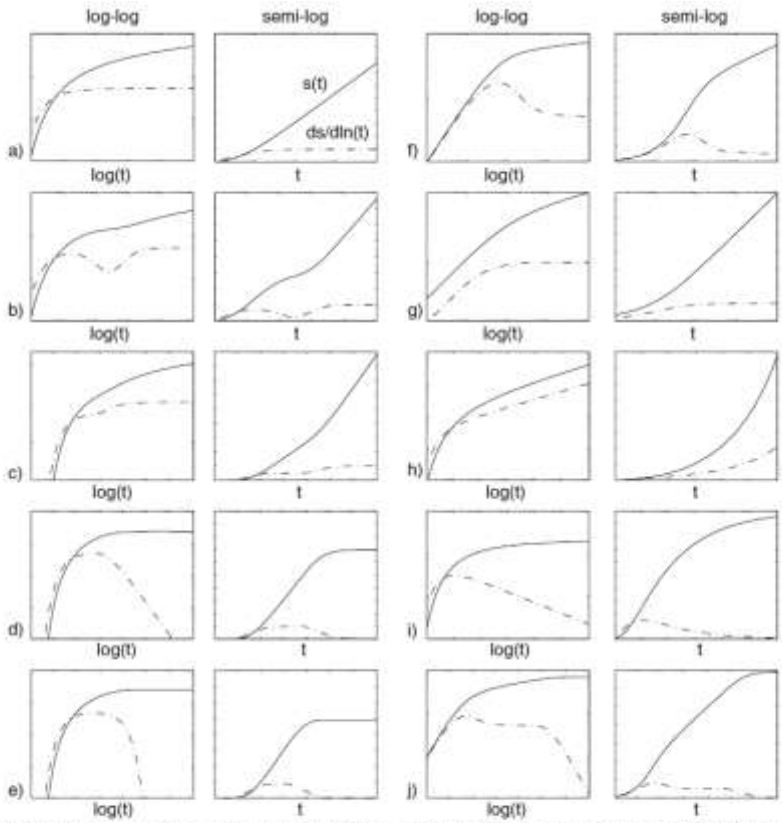

Fig. 2 Most typical diagnostic plots encountered in hydrogeology: **a** Theis model: infinite two-dimensional confined aquifer; **b** double porosity or unconfined aquifer; **c** infinite linear no-flow boundary; **d** infinite linear constant head boundary; **e** leaky aquifer; **f** well-bore storage and skin effect; **g** infinite conductivity vertical fracture.; **h** general radial flow—non-integer flow dimension smaller than 2; **i** general radial flow model—non-integer flow dimension larger than 2; **j** combined effect of well bore storage and infinite linear constant head boundary (modified from Renard 2005b)

Figure 2.5.3 Diagnostic plots for pumping tests (Renard *et al*. 2008)

The plots presented in figure 2.5.3 are the most frequently encountered in hydrogeology (Renard *et al*. 2008) and serve as useful guides when choosing the analytical solution and are good indicator for the different flow regimes surrounding the pumped well. They consist of the drawdown data which is denoted as s (t). It also consists of the derivative plot, which is ds/d ln (t). The derivative plot is often used for finding boundaries when pumping, e.g. constant head boundary in an unconfined aquifer (Renard *et al*. 2008).

3 MATERIALS AND METHODS

3.1 Aquifer observations and maps

The aquifer water level was observed with submerged data loggers in observation wells from 24.10.2010 to 10.11.2010. Precipitation was measured with a pluviograph installed near the observation wells.

The GR02 well was observed and data logging devices was submerged in the water to measure the fluctuations in hydraulic head as a response to environmental factors as the barometric pressure and the tidal activity. This well is located approximately 120 meters inland from the southern coast. The data recording device is a data logger which records change in centimeters of water above the sensor. This includes the weight of the column of air above the well. To correct for the barometric effect, a barometric logger was installed in the same well, above the water table. This records the column of air above the logger (in cm water), so to find the correct water level in the well, the weight of the barometric pressure has to be subtracted.

Figure 3.1.1 Location of observation loggers and wells.

The map presented in figure 3.1.1. shows the locations of the *in situ* data loggers, and the wells used for the pumping tests.

For tidal fluctuations near the aquifer, a data logger was placed in the contact with the sea at the south pier (the SVR01 location). To prevent fine grained material to enter the pressure transducer; and to ensure minimal horizontal and vertical movement of the logger, the device was placed in a perforated PVC tube which was then installed vertically in the ocean. This is shown in figure 3.1.2 along with the GR02 data logger.

Figure 3.1.2 Tide observation point and the GR02 barometric observation device

The submerged data logger also recorded the electrical conductivity of the water in the well. This is presented as micro Siemens per centimeter. All water levels have been corrected to the same reference datum, the NN1954. The accuracy of the divers were reported to be within +- 0.5 cm. The results from this observation are presented in figure 3.1.3.

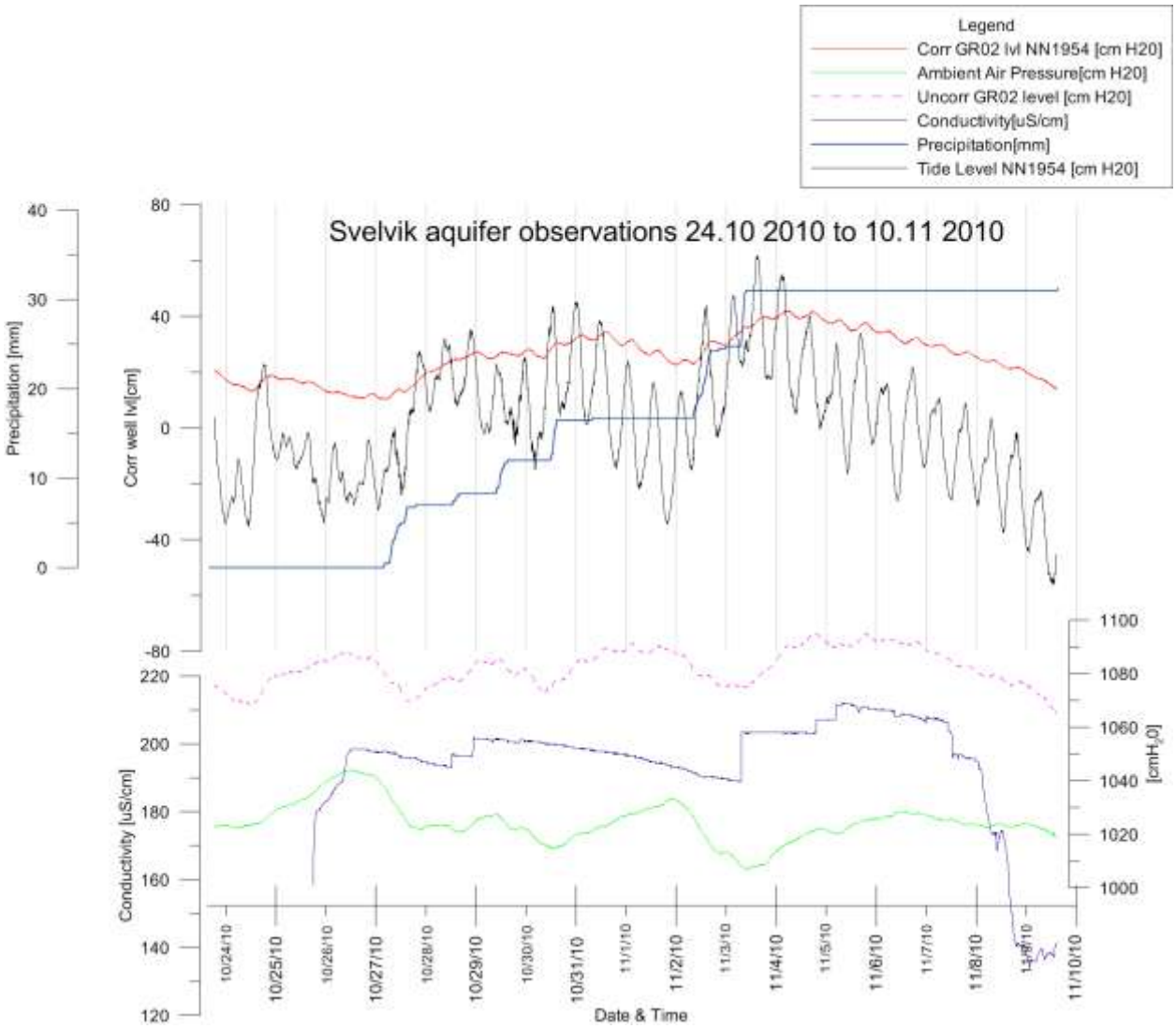

Figure 3.1.3 Aquifer observations

The results of the aquifer observations indicate a good correlation between the hydraulic head in the well and the tidal level measured in the fjord. The oscillation of the water level in the well is indicative of transient groundwater flow conditions. These observations will be used for the estimation of hydraulic diffusivity based on the Ferris method.

The air pressure has a distinct impact on the water level, as it is expected in unconfined aquifers (Driscoll 1986). This can be seen from the similarities in the uncorrected GR02 well level and on the air pressure graphs. The air pressure has a higher impact on the water level in the well than the tidal oscillations. The uncorrected water level fluctuates with approximately 40 centimeters from troughs to peaks in the graph, whereas the corrected level only fluctuates 2-3 centimeters diurnally and approximately 20 centimeters weekly.

Connected with changes in air pressure is the precipitation. As expected any precipitation infiltrates rather quickly and contributes to the ground water level, as can be seen from the rapidly rising water levels after precipitation.

3.2 Electrical methods

3.2.1 Data acquisition

Four lines with 72 electrodes with 3 and 5 meters spacing were deployed on several days in mid-September 2010. The electrodes were deployed successfully and except for the first line, C-C', the resistance between each electrode was lowered to less than 13 kohm. This was done with "watering down" the electrodes with an electrolyte solution.

The weather was clear and sunny for all days of measurement, with no or little precipitation for the previous week. This might have dried out the unsaturated zone significantly and subsequently lowered the conductivity for the top layer.

Abandoned and buried pipes and tubes along with blasting cable were seen buried around. This might influence the results as buried metal objects can distort data, especially if the conductive body lies in such a way that the electric current will prefer to pass through it instead of the adjacent soil.

Figure 3.2.3 shows a steel electrode inserted in the ground, connected to the multi-electrode cable. The electrode was hammered down approximately 20 cm in the ground. There were some challenges due to topographical features to keep the electrodes in a straight line.

Figure 3.2.3 Electrode in ground

Figure 3.2.4 The Switch connected to battery

Figure 3.2.4 shows the programmable switch hooked up to the ground electrodes and external power source. The external power source was a 12V car battery.

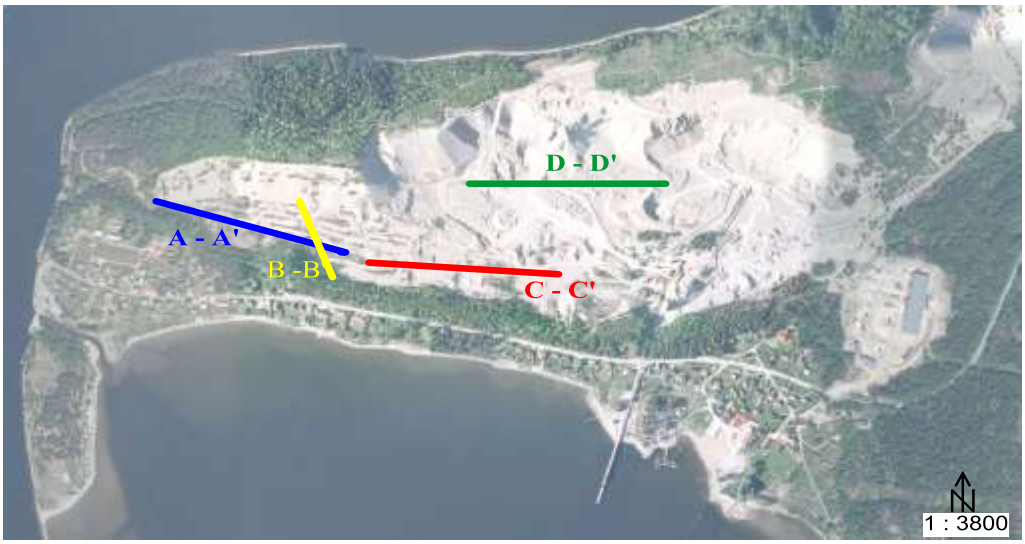

Figure 3.2.5 Location of the resistivity lines

The locations of the lines were selected in the field from topographical limitations and the possibilities for 360 meter long surveys along a relative straight line. There were no major problems during acquisition.

3.2.2 Data processing and filtering the report point distribution graphs

The creation of the models follow a three step procedure. It can be summarized as follows:

- Creation of report point distribution based on the data obtained. This was then filtered witht he Prosys application to eliminate most of the bad data points, and to inspect the quality of the data set. Topography was implemented in the models at this point. This eleveation data was based on maps and a quick visual survey along the lines.
- The pseudosections was then imported in the RES2DINV application. Then it was filtered further by eliminating the few bad data points which were missed during the filtering.
- Lastly the the inversion was perfromed which created the models based on the filtered pseudosections. The paramters used was robust inversion and a horizontal / vertical filter of 0.5.

The most used filter was to eliminate any negative apparent resistivity values and zero values. The two others were to elimatate any report point which were obviously wrong, either too high or too low values. The sliding avaerage filter to lower the extreme values for noisy data sets, this was done not to remove too many report points. Some of the pseudosections were reduced vertically as the deepest values were very noisy.

The following report point distribution gives an insight of how the apparant resistivity values are distributed. The values should be used for interpretation. It does however, give an insight of the data quality and amount of noise present. This is an intermediate result and is therefore presented in this section.

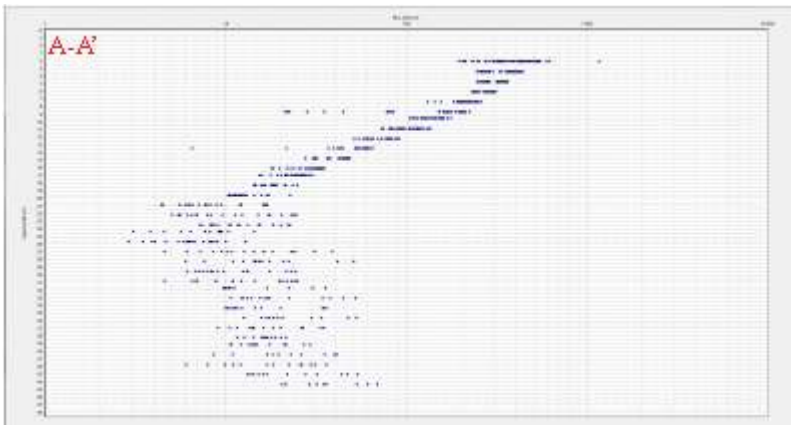

Figure 3.2.6 AA' report point distribution

Figure 3.2.6 shows an increasing variation towards deeper measurements. This may be attributed to several factors including noise, heterogeneity of the depth or faulty electrodes.

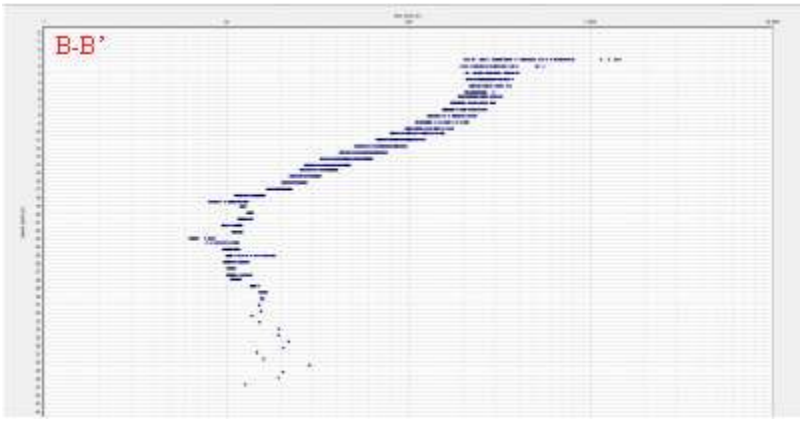

Figure 3.2.7 BB' Report point distribution

The B-B' line presented in figure 3.2.7 has a smaller electrode spacing (3 meters) so the resolution is higher, but the depth penetration is lower. This data set had less noise and was subsequently not filtered much. However, there were large resistance variations in the top layer; this is easily seen from the top distribution. This was expected since the lines crossed small piles with coarse gravel.

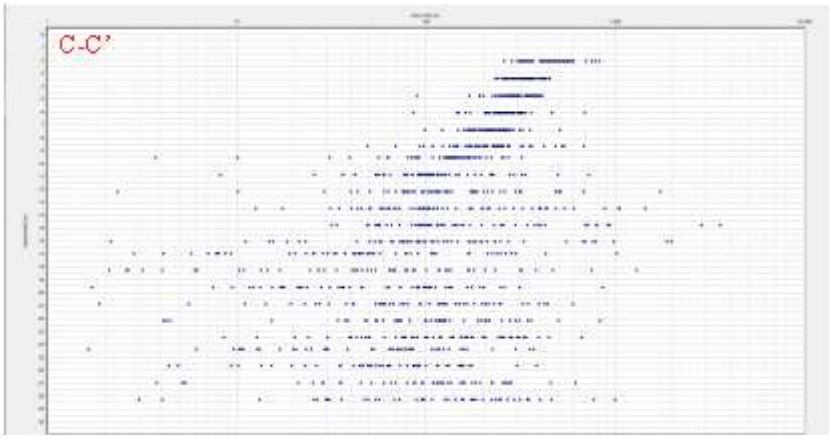

Figure 3.2.8 CC' Report point distribution

The C-C’ line in figure 3.2.8 was by far the noisiest data set as can be seen from the report point distribution graph. This was along the main road, and blasting wires and pipes were observed near the lines. This was also the first measurement done, and the electrodes were not watered down with sea water, so ground electrode resistances were very high. The data set had also several negative apparent resistivity reference points, which is omitted in the report point distribution.

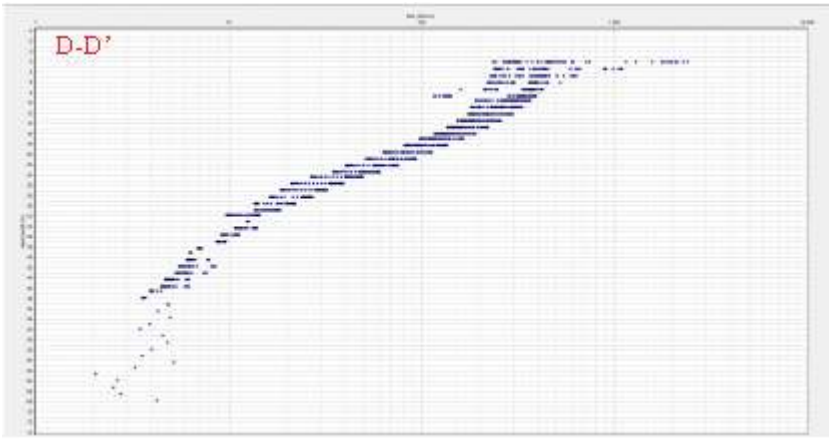

Figure 3.2.9 DD' Report point distribution

The D-D’ set presented in figure 3.2.9 was the least nosy data set of all. This is in the newly exposed area and thus it has not been subjected to much anthropogenic activity. The mid-section of the upper layer is highly resistive; this was can be attributed to a hill top with coarse sand and gravel. The lower parts show a more wide spread distribution. This line was measured in a newer exposed area and more in the middle of the deposit (figure 3.2.5)

These data sets were filtered and inserted into the inversion application RES2DINV and the resulting models are presented in section 4.2.

3.3 Tidal Forcing method

Based on the fluctuations on presented in figure 3.1.3 the Ferris' tidal forcing method described in section 2.4 has been applied.

3.3.1 General description and power amplitude spectrums

As can be seen in the graph from the aquifer observation there is a good correlation between the tidal level and the head measured in the GR02 well. The phase shift between the two signals can clearly be seen from the graph. There are several ways to obtain the characteristics of each cosine, for this test the Fast Fourier Transform will be used.

For this data series the total number of readings was 4848 sampled at 300 seconds intervals. The FFT fits N/2 frequencies to N data points, for this series this means 2424 frequencies in the frequency domain.

For this study, the sampling interval is 300 seconds, so the Nyquist frequency is 1.7 mHz, and subsequently the Fourier transform will contain information from 0 Hz to this frequency. The lunar semi-diurnal constituent M_2 has a period of approximately 12.41 hours (Defant 1961) so 5 minute sampling interval should be adequate to resolve the desired tidal frequencies.

The mean value of the data set was removed with the Matlab's detrend function to eliminate a peak at 0 Hz on the amplitude spectrum. The amplitude spectrums were produced by plot the amplitude for one side of the amplitude spectrum on the y axis and the x axis denotes the frequency range from 0 to the Nyquist frequency in Hz. The spikes indicate more energy at the given frequency, and the known periodicity of the tidal constituents can be compared to this graph. The amplitude spectrums are presented in figures 3.4.1 for the tidal observation and 3.4.2 for the inland well GR02 observation.

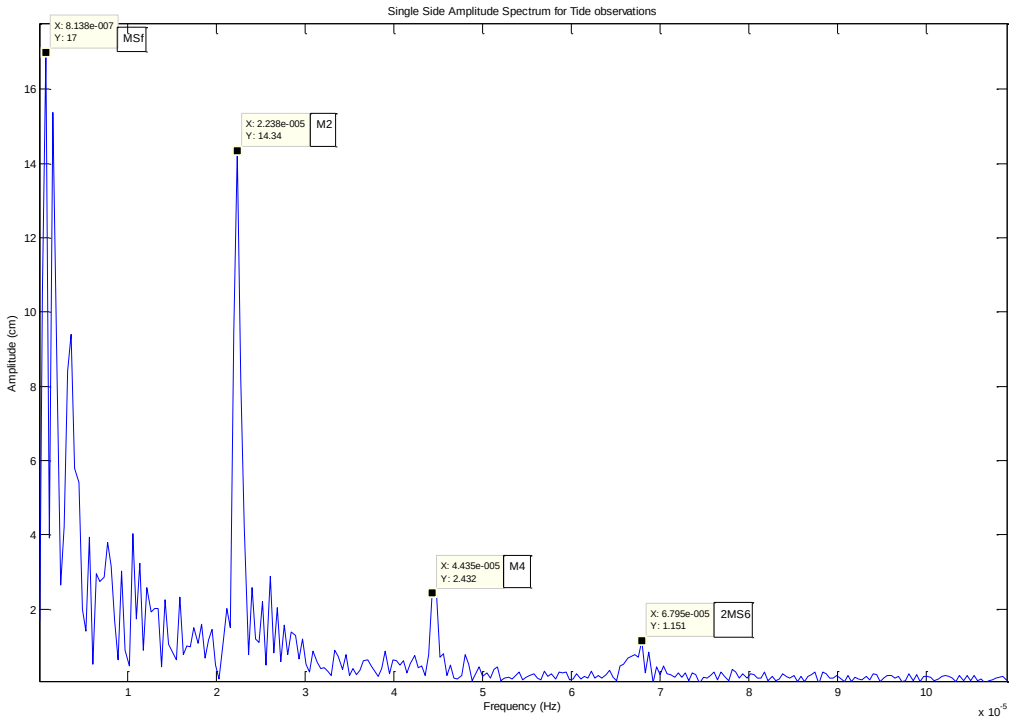

Figure 3.4.1 Amplitude Spectrum of tide

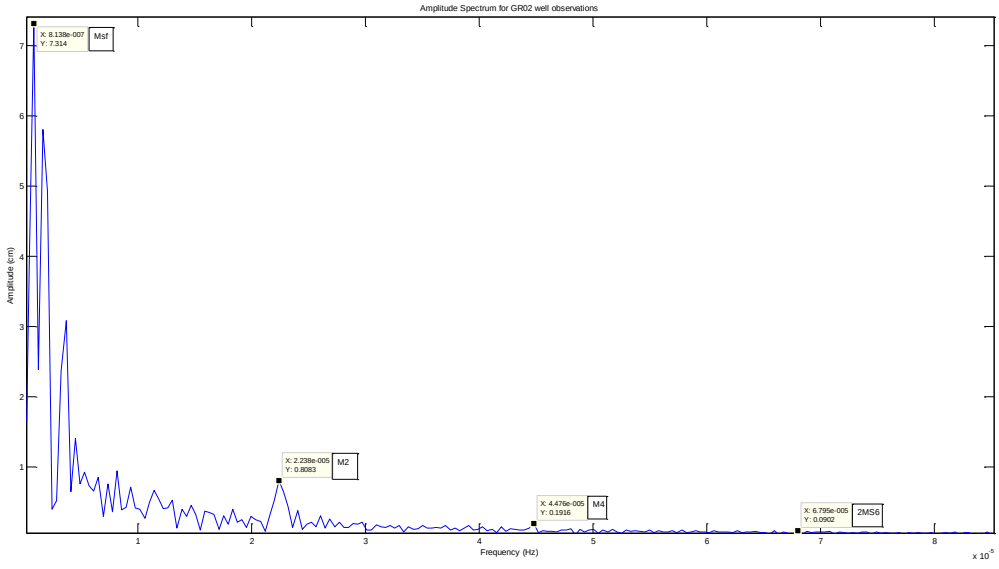

Figure 3.4.2 Amplitude Spectrum of GR02

3.3.2 Identification of tidal constituents

There are several spikes which are both discernible in both the tide and well observations. However the two frequencies with the largest amplitude in the tide are the M_{sf} constituent and the M_2 constituent. The M_{sf} constituent has a period of 14.75 days, the measured one here has a period of 14.24 days (Jarosz 1997). There might be complicating factors such as the sea bed topography and the nature of the deposit, which function as a barrier between the inner and outer basin. However, for this test this is identified as the M_{sf}.

The M_2 constituent which has a period 12.42 hours adheres quite well to the expected period of 12.41 hours (Defant 1961).

The other spiked frequencies does not seem to fit any of the known tidal constituents, and may be attributed to complicating factors as weather systems, bathymetrical conditions or the tidal current Svelvikstrømmen's influence.

3.3.3 Lag and Efficiency results from the FFT

Table 3.3.1 shows the calculated lags and amplitude losses for the different constituents based from the Fourier analysis. The M_4 and $2M_{S6}$ constituents, the response in the well were so low that it may be regarded as noise and subsequently these constituents will be omitted from the rest of the experiment.

Table 3.3.1 Lag and Phase from the FFT

Frequency(Hz)	Period (s)	Constituent	Phase lag (rad)	Efficiency
8.14E-07	1.23E+06	M_{Sf}	-0.26	0.43
2.24E-05	4.47E+04	M_2	-1.18	0.06
4.35E-08	2.30E+07	M4	0.49	0.08
6.80E-05	1.47E+04	2MS6	-0.79	0.08

The amplitude is much lower in the observation well for the M_2 constituent, and the ratio is 0.06 which is very low compared to the ratio for the M_{sf} which is 0.43.

3.4 Pumping test

3.4.1 Description of the procedure and details surrounding the test

The pumping test was performed by NGI during August 16th and 17th 2010. The BR03 (see well map) well was pumped with 3" submersible pump (Grundfos SQ/SQE 2-70) (Kristjansson 2010). The abstracted water was dumped 170 meters away from the well to prevent re-infiltration.

When performing a pumping test it is commonplace to perform a step-drawdown test. This is done to ascertain the well characteristics. This has not been analyzed for the use in this thesis. For a complete description and results of the step drawdown test performed before this pumping test see Kristjansson (2010).

For this pumping test the distance between the pumping well and the observation well GR08 is 4 meters. The pumping rate is assumed to be at a constant 0.7 throughout the whole pumping period. For the observation well measurements the pressure transducers were installed in all well surrounding the BR03 (pumping well) during the test, so they all registered the drawdown in each one of them. For this test, however, the GR08 well be used as the observation well.

The penetration depth for the BR03 well has been measured to be 6.6 meters depth, and the GR08 is 6 meters deep. The aquifer base, as established from the geophysical measurements is between 7-30 meters, and different bases will be tried when applying the analytical models. For an exhaustive description of the wells see Kristjansson (2010).

This pumping test was influenced by precipitation after 15 000 seconds, and the recovery was also influenced by precipitation. This pumping test will be based on the first 15 000 seconds.

The observed drawdown in the GR08 well is portrayed graphically in 3.4.1. For the other figures 3.4.2 - 3.4.4 is presented with different values on the axes and also contain a derivative plot (the red crosses).

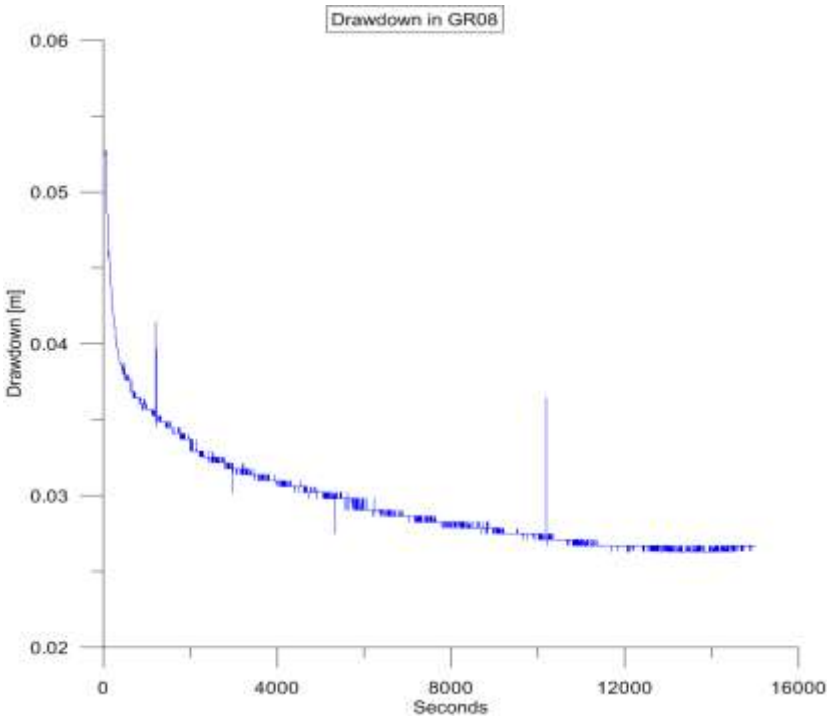

Figure 3.4.1 Drawdown in GR08 during pumping

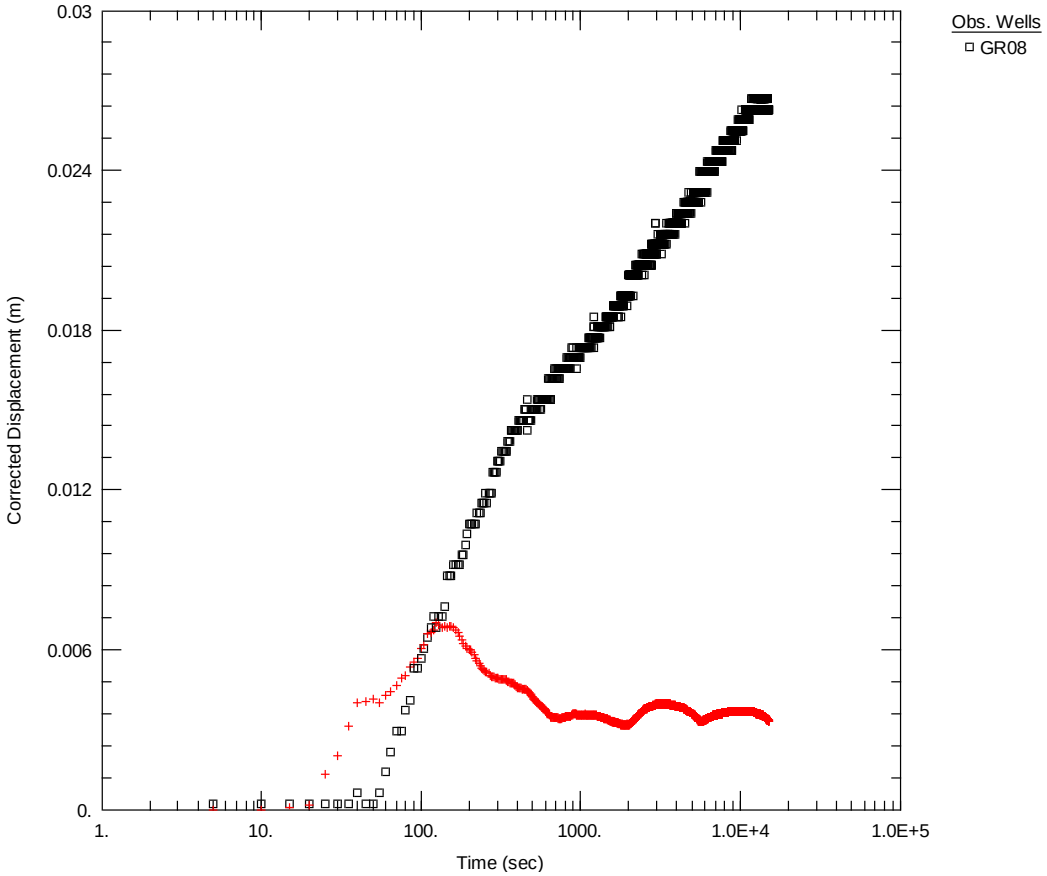

Figure 3.4.2 Linear-log plot GR08 (Red line is derivative plot (Spane 0.7)

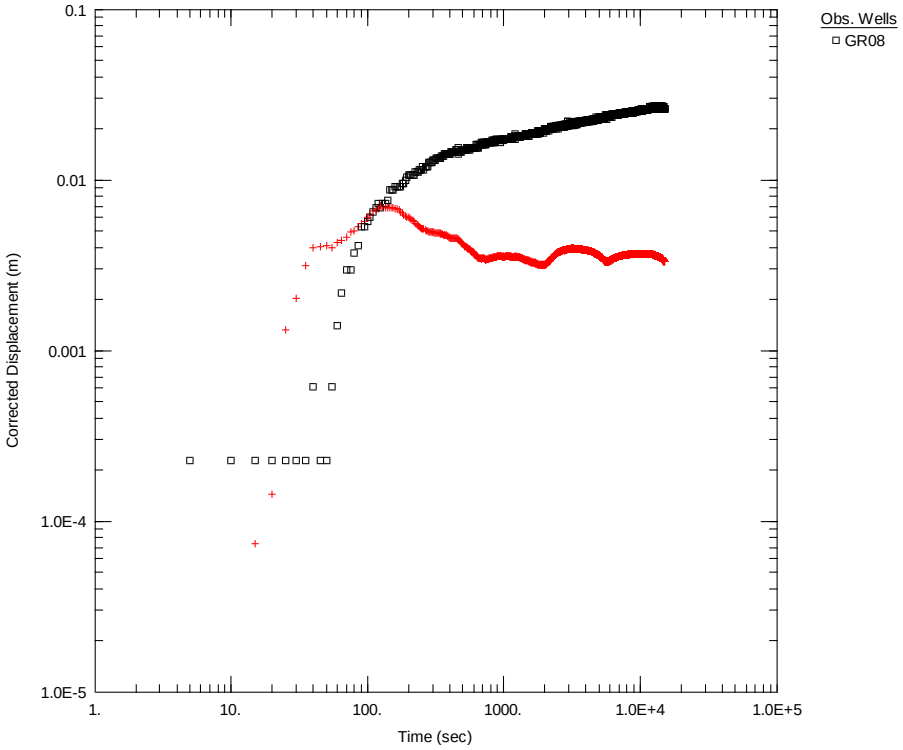

Figure 3.4.3 Log-Log plot GR08 (Spane 0.7)

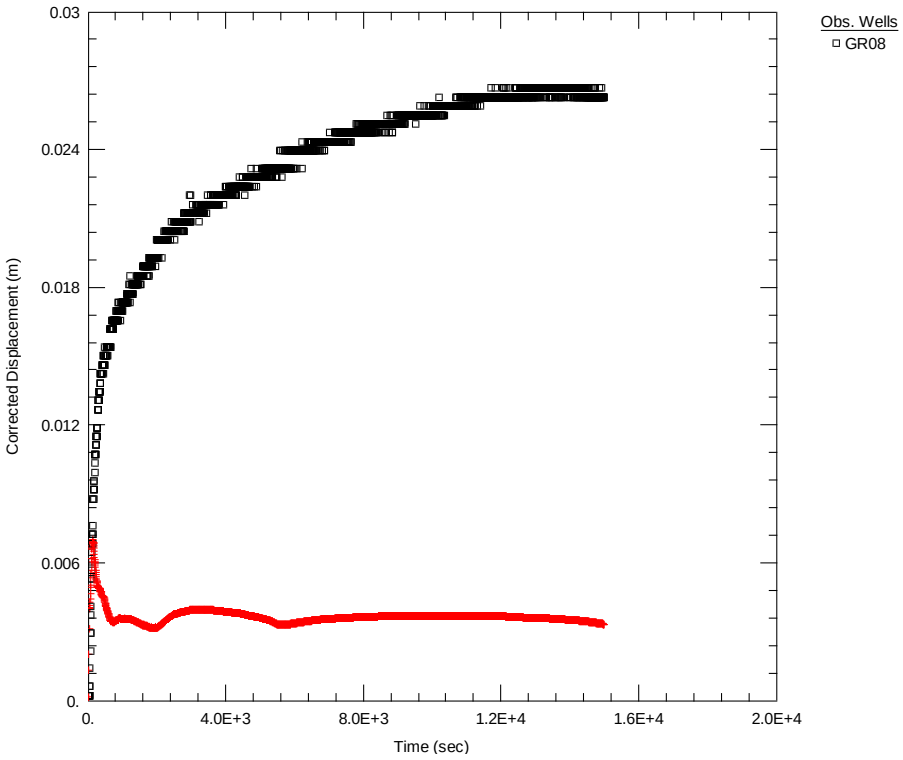

Figure 3.4.4 Linear-Linear plot GR08 (Spane 0.7)

The diagnostic plots are presented in figure 2.5.3. These are important tool for determining the different flow regimens and thus which analytical model is applicable (Krusemann and de

Ridder 1992). For this test the radial plot was used to determine any delayed gravity response, which is often observed in unconfined aquifers. This can be observed as a curve at intermediate time (comparable to figure 2.5.3b). Further it is possible to see if the aquifer has infinite-acting characteristics by observing a straight line at late time (figure 2.5.3c) which is one of the Theis assumptions (Krusemann and de Ridder 1992).

The pumping test drawdown curves in figure 3.4.2, 3.4.3 and 3.4.4 compared to the various diagnostic plots in figure 2.5.3 and suggests that the flow regime are mainly influenced by:

- Unconfined aquifer (B)
- Infinite linear no-flow boundary (C)
- Well bore and skin effect (F)

The unconfined aquifer is diagnostic is not very well pronounced, as can be seen from the derivative graphs. The easily recognizable drop in this graph (figure 2.5.3b) is not easily seen in the pumping test graphs. It may however, be overshadowed by the well bore storage and skin effects, as indicated in figure 2.5.3f. The infinite no-flow boundary compares (figure 2.5.3c) well to the pumping test data showing a straight line at the late data.

The wellbore skin effect is used to account the difference between the measured and predicted drawdown. The skin which is a result from altered permeability around the wellbore can be positive or negative (Krusemann and de Ridder 1992). For the positive effect the interface between the aquifer and the well is damaged. This lowering of the permeability around the bore can be the result of mud infiltration during drilling; clogging the screen by coarse particles; some sorts of mineral precipitation or improper screen size. The negative skin effect is less encountered and may take place where the permeability around the well is enhanced, this may stem from acid precipitation or hydraulic fracturing (Krusemann and de Ridder 1992).

The shallow well was drilled with bentonite mud, and subsequently the mud may have entered the formation and altered the formation's characteristics around it.

4 RESULTS AND DISCUSSION

4.1 Lithologic log

The lithologic log presented in figure 4.1.1 is based on flush samples from a drilling operation in 1981 (Sørensen 1981).

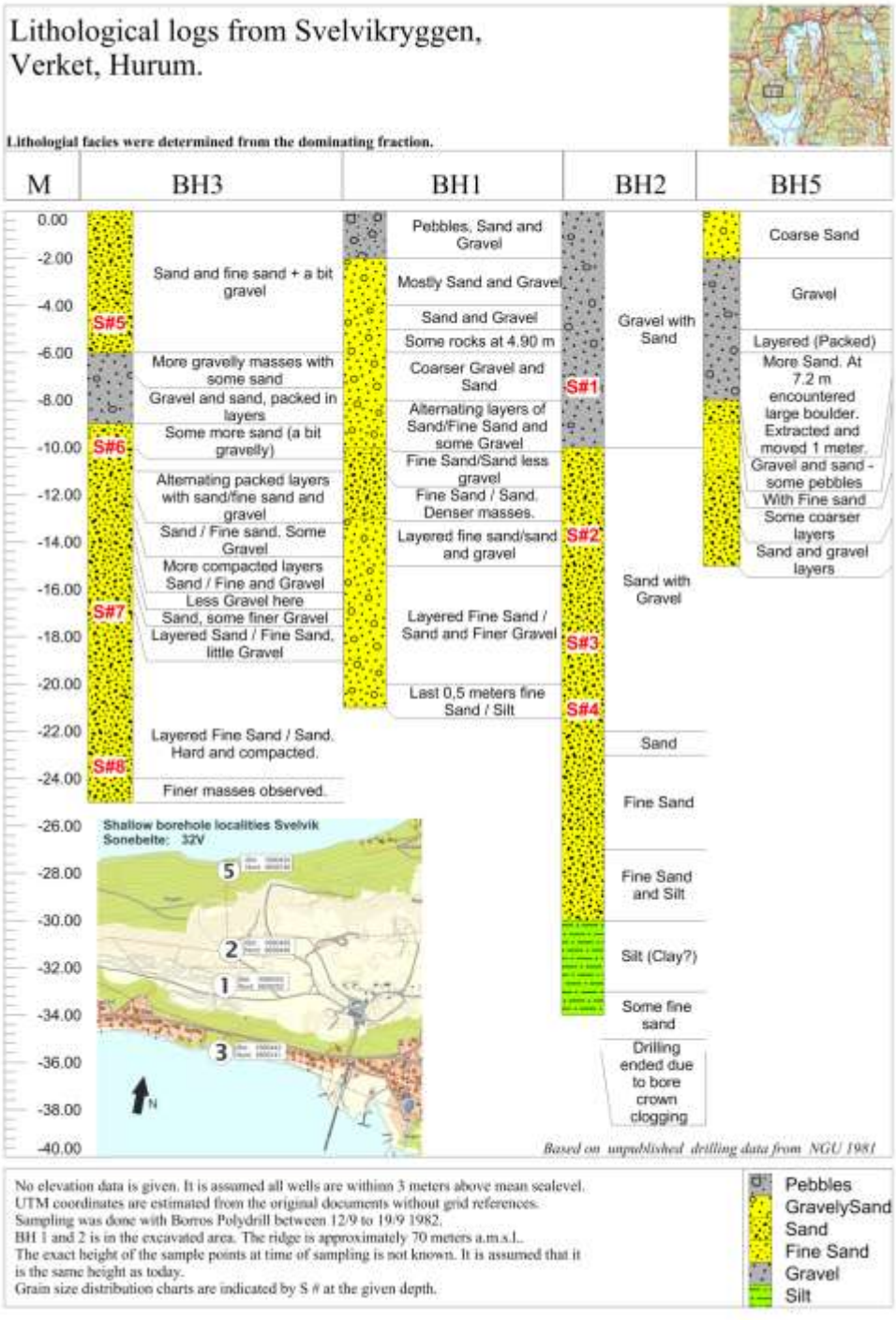

Figure 4.1.1 Lithologic log from Svelvik Ridge (Based on unpublished data Sørensen 1981)

A general trend of fining sediments as depth increases is observed, the shallow BH5 is exempt from this trend. At around - 30 meters in BH2 a silt or clay layer was encountered, enough to clog the bore crown. This suggests a clay layer at around that depth, however this was not confirmed when drilling the 300 meter deep well in the summer of 2010. The presence of clay can serve as a possible confining or retarding layer. However, the other boreholes suggest finer sediments from around -20 meters, and the first silt / very fine sand is encountered shallower in BH1 at around -10 meters. Lenses with different sediments are expected in glaciofluvial deposits, and was frequently encountered in the Storsand deposit (Lønne 1993). In BH3 from -6 to -9 meters may be an example of a gravel lens.

Since no real elevation data was given in the data descriptions, it is assumed that the topography has not changed significantly during these 30 years. A map which came along with the unpublished drilling data supports this. However, a land survey should be done where the boreholes are to establish the height relative to the NN1954 datum. This was not done here and the depths should then be considered as tentative.

The lithologic log should only be used as an indicator of the changes in lithology, and the depth to the confining layers should be complemented with other geophysical methods.

The grain size distribution charts are presented here in the results section as they are a part of the resulting lithologic log presented.

4.1.1 Grain size distribution charts and hydraulic conductivity estimates

Based on these grain size samples the hydraulic conductivity values has been estimated based on the Hazen (1893) and Gustafson (1984) method presented in section 2.2.7.

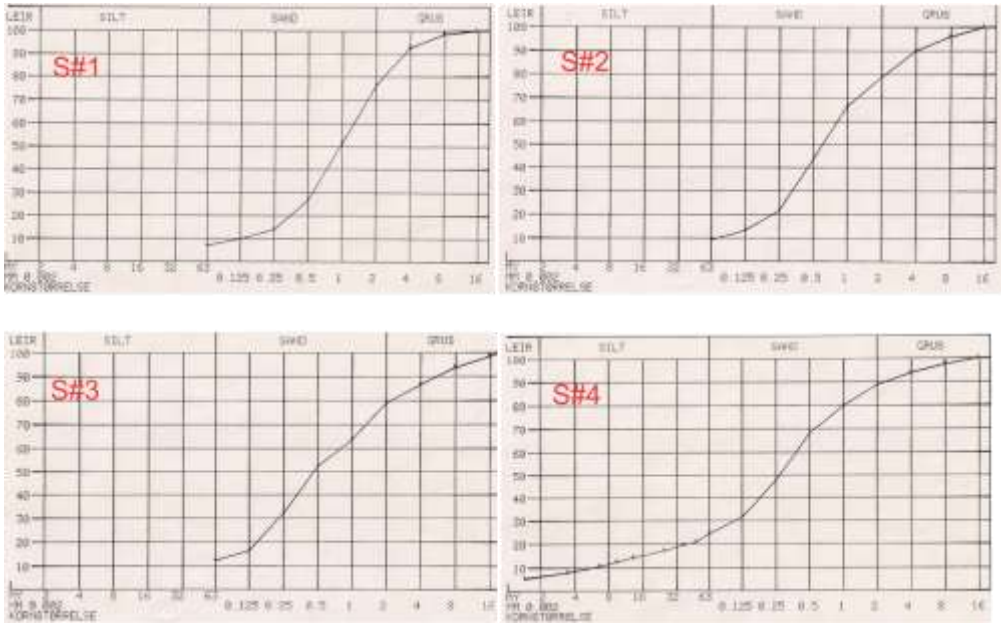

Figure 4.1.2 Grain size distribution from BH2

Figure 4.1.3 Grain size distribution from BH3

Two methods described in section 2 were used to estimate the hydraulic conductivity in BH2 (Table 4.1.2) and BH3 (figure 4.1.3). The Hazen and Gustafson method was used as described in section 2.2.7. These gave slightly different results, the Gustafson method yielded lower values in general than the Hazen method.

Table 4.1.2 Hydraulic conductivity estimates BH2

BH2		
Depth (m)	Hazen(m/s)	Gust(d50) (m/s)
7	1.81E-04	1.53E-04
14	4.49E-05	3.56E-05
18	4.49E-05	3.56E-05
21	2.89E-07	6.57E-08

Table 4.1.3 Hydraulic conductivity estimates BH3

BH3(m/s)		
Depth (m)	Hazen(m/s)	Gust(d50) (m/s)
5	4.63E-04	6.28E-04
10	2.89E-03	2.79E-03
17	4.59E-05	5.58E-05
24.5	6.12E-08	7.73E-09

The hydraulic conductivity estimates from the empirical formulas (section 2.2.6) for BH2 between 18 and 20 meters is lowered by the presence of the silt/clay fraction. This reduces the hydraulic conductivity estimate to 0.01 md^{-1}. This is classified as impervious by Bear (1979) and flow velocity falls in the clay / silt range. For the BH3 at 24 meters depth the hydraulic conductivity is even lower, and falls also in the clay / silt range. Based on these two observations there is a trend with finer sediments with increasing depths.

The mid and upper sections of the aquifer have hydraulic conductivity estimates from 3 to 241 md^{-1}. The wide range of this may be attributed to anisotropy or the method used when obtaining the samples. Bear (1979) classifies these values as good to poor aquifer characteristics with sand and gravel for the higher values and VF, silt and loess for the lower values.

The grain size distributions are based on flush samples, and should be treated accordingly. The samples should be used with caution and the drilling method and sources of error should be made aware of. Details from the drilling operations are not available, except what is presented on the log (fig 4.1.1).

Perers (Gustafson *et al*. 1984) conducted a study of flush samples and the grain size distributions in glaciofluvial material in Southern Sweden. He found that flush samples and samples obtained from rotational drilling differed from an actual sample from core sample. This was attributed to the quality of the samples and systematic errors. In general the conclusion was that samples obtained with apertures at the end gave a more realistic sediment distribution than the samples obtained with side apertures. For the side holes method the coarse grains was overrepresented. Samples obtained from drilling should be considered carefully, and only be used as guides since they do not represent the actual sediment composition (Gustafson et.al 1984).

Other factors include the aperture of the screen and the flush pressure (Gustafson et.al 1984). However, none of this information were available and the values obtained from the samples should be treated only as what they are estimates. This is promoted further by the use of empirical formulas, which also contribute to a higher degree of uncertainty.

4.1.2 Conclusion on hydraulic conductivity estimates

The values show that with depth the hydraulic conductivity decreases. The for the BH2 between 18 and 21 meters the value are very low and is described by Bear (1979) as impervious. The same is for BH3 between 17 to 24.5 meters. Further work to establish the basement of the aquifer has been done by the electrical resistivity tomography method presented in the next section.

4.2 Electrical resistivity models

The data from the inversion routines generated the following resistivity models. Three models are oriented from West to East and one, the BB' model, is slightly oblique to the North-South direction. The AA' line intersects the BB' line at the indicated point.

All figures follow the same setup, beginning with the measured pseudosection at the top. This is the result after filtering the raw data sets shown in the report point distribution figures. The middle figure is the calculated pseudosection. The lowest figure is the inverted resistivity model which can be interpreted geologically.

4.2.1 A-A' line Model

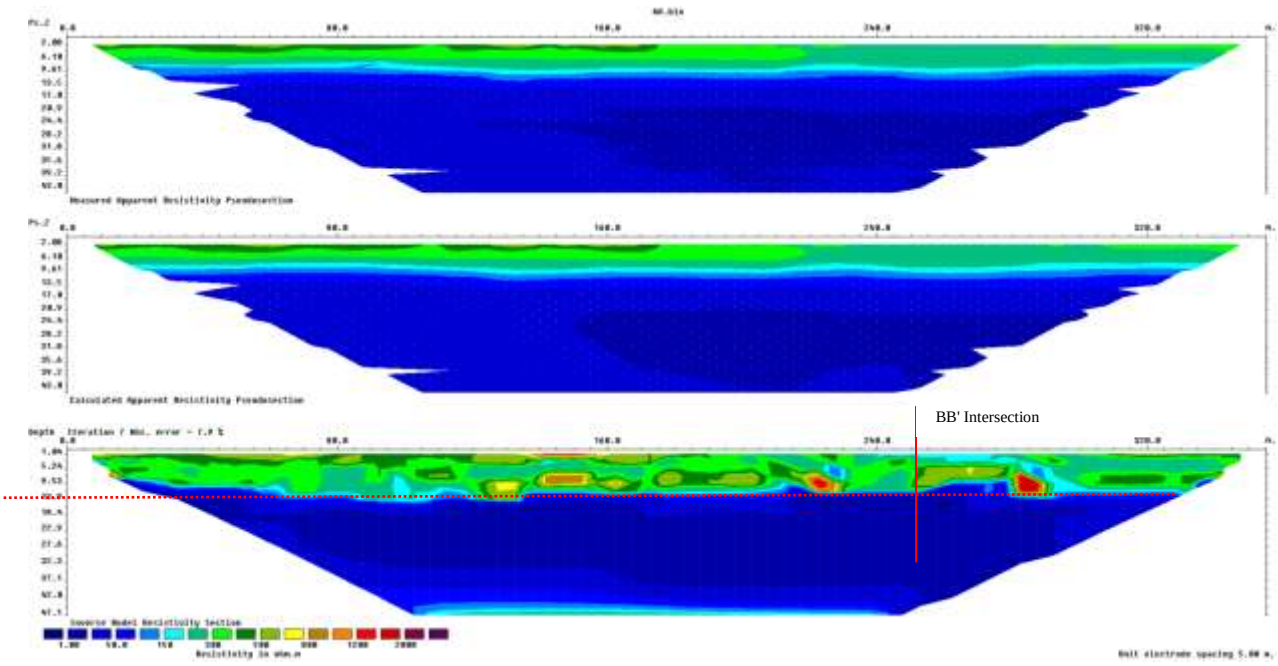

Figure 4.2.1 AA' line inversion and resultant model

An obvious feature of the AA’ model in figure 4.2.1 is the two layers characteristic. The model is separated at circa 14 meters (the red dotted line) with a relatively homogeneous lower layer with resistivity values varying from 2-30 ohmmeters. Higher values can be seen at the lower parts of the model.

For the heterogeneous upper layer the values range from 100 to several thousand ohmmeters. In the top layer there are angular lenses with higher and lower values than the surroundings. The most prevalent value is 200 to 400 ohmmeters, however some areas in the model shows ranges upwards to 2000 ohmmeters. Higher values can be observed closer to the surface.

4.2.2 B-B' line Model

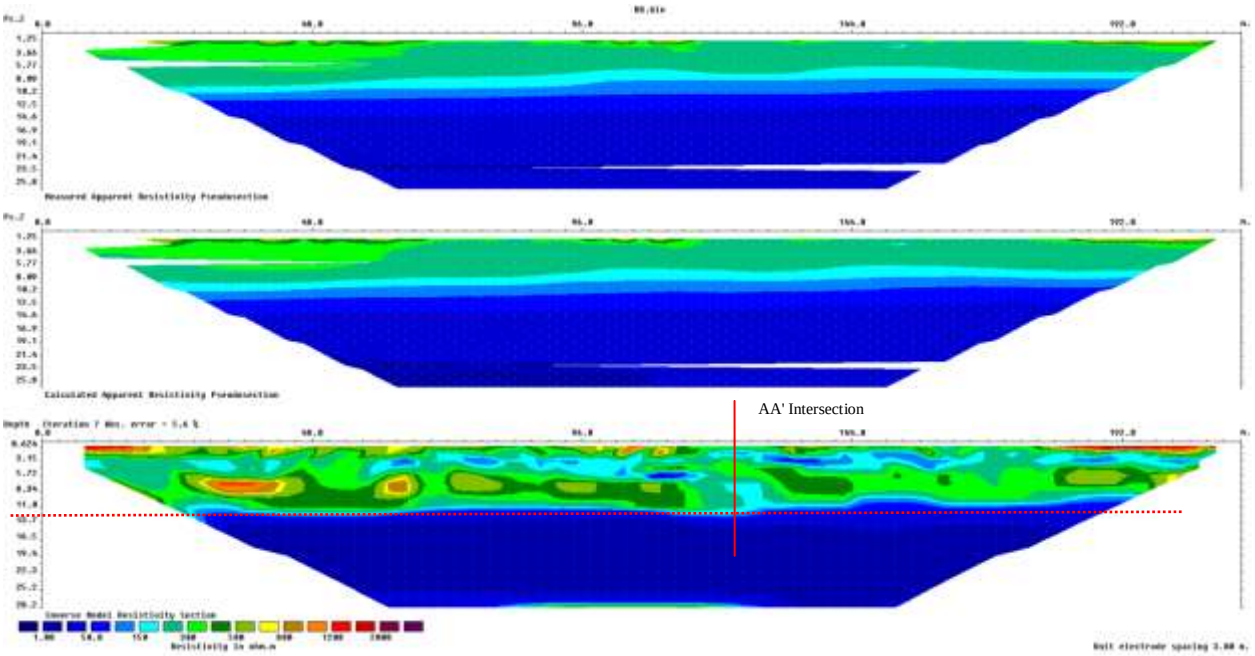

Figure 4.2.2 BB line inversion and resultant model

The BB' line in figure 4.2.2 has a higher vertical resolution as a result of a smaller electrode distance.

The intersection point between the two readings similar values and depths to the interface between the layers are present.

The two layer characteristics of the subsurface can be observed in this line as well. This line has a more North South orientation, and the model reveals a dipping feature of the two layers. The same resistivity values of the lower layer can be seen, and the heterogenic upper layer spanning from the thousands to the lower 5-10s ohmmeters is present.

A notable feature of the upper layer is that there seems to be a lower resistivity band from ca. 3 to 5 meters depth. This is followed by a higher resistivity area in the 300-500 ohmmeters range.

4.2.3 C-C' line Model

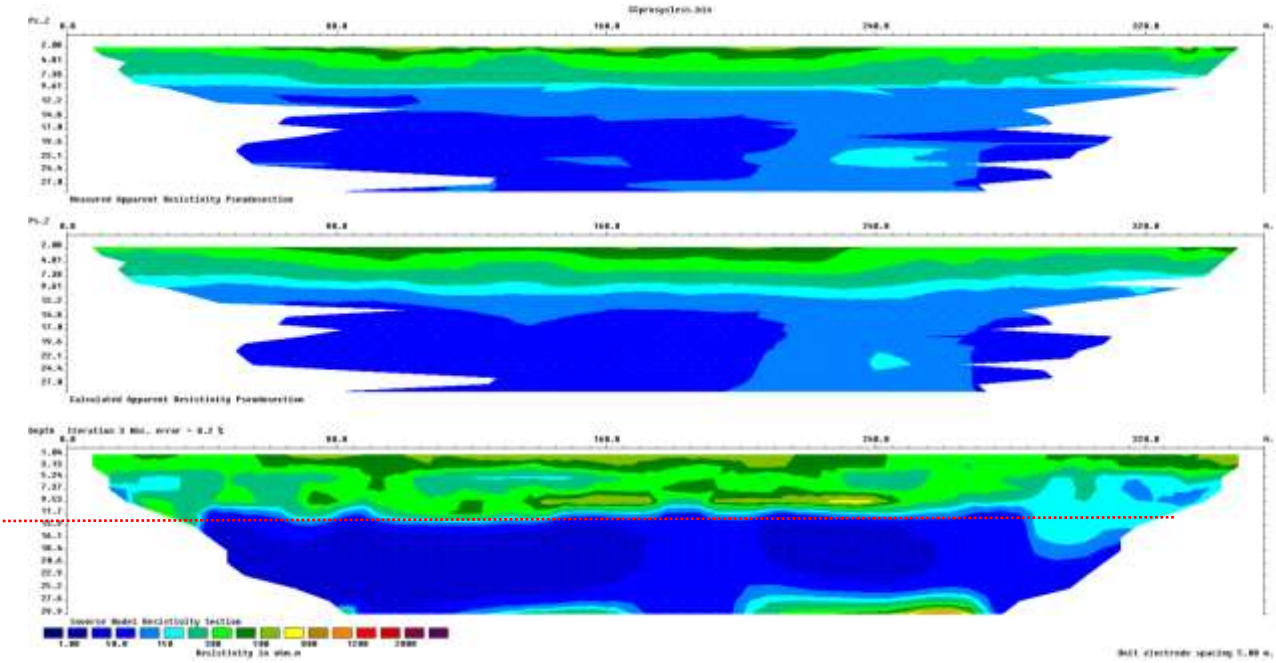

Figure 4.2.3 CC' line inversion and resultant model

The CC’ model in figure 4.2.3 was heavily filtered, this can be seen in the pseudosection with the blanked out areas. A sliding average filter was applied and this evened out any large variations in the upper part. The removal of bad data points was mainly done in the sides, and in the deeper parts, so this model has a reduced reach down to about 30 meters. However, the two layer structure is still recognizable divided at the approximately the same depths as the other models.

The top layer has less heterogeneity than the other models, and the lower layer indicates the same values as the other models. The eastern side shows an anomalous area reaching down to 20 meters. At the lower end of the second layer there are areas with higher resistivity values.

4.2.4 D-D' line Model

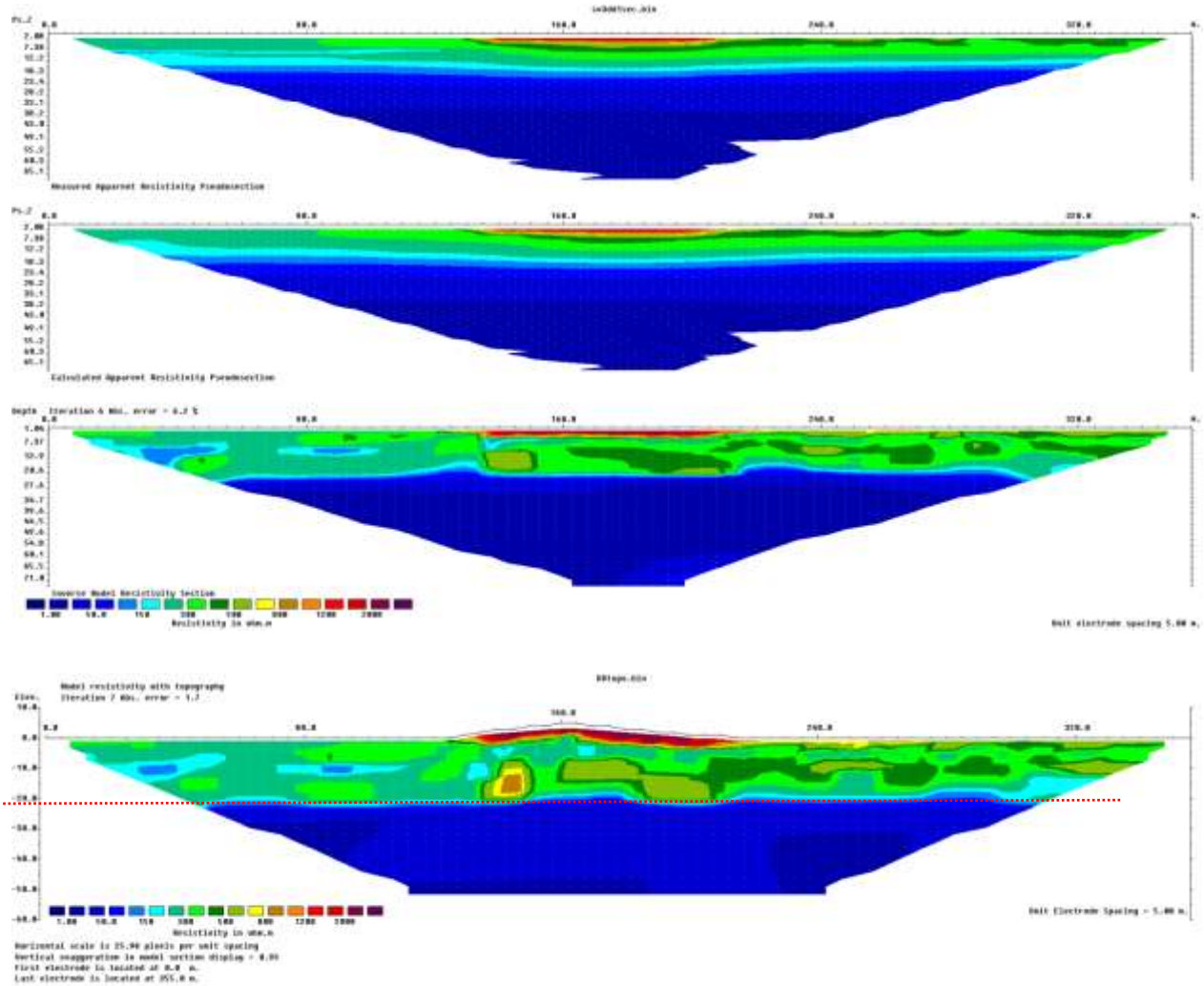

Figure 4.2.4 DD' line inversion and resultant model

This area was the only with any significant topographical features. This resulted in a second model with topography presented in figure 4.2.4. The topography had an impact on the resultant model, and some of the specific resistivity values changed significantly. However, still a two layered subsurface can be seen but at a different depth than the other models. The interface occurs at ca. 21 meters.

In the middle of the model, from 100 to 200 meters a hill with high resistivity values up to 2000+ ohmm can be seen. The heterogeneous top layer is found here as well, however, it is deeper than the other models.

The more homogenous lower layer has resistivity values ranging in 5-20 ohmmeters.

4.2.5 Discussion and comments on the resulting models

All models illustrate the easily recognizable subsurface layers with different electrical properties. However the depth to this interface should be interpreted critically and there are several sources of error when measuring and when modeling the results. It is further easy to make mistakes in the interpretation of these models owing to the principles described in section 2.3.

The dipole-dipole method used here is not particularly sensitive to vertical changes in ground resistivity (Reynolds 1997), but should be adequate to resolve any subsurface layering (Solberg *et al*. 2011). A more insightful method could be the gradient array or a Wenner/Schlumberger configuration, which is more sensitive to vertical changes in electrical properties (Solberg et.al 2011). However, for this thesis the dipole-dipole was chosen mainly due to great penetration depth of the method and partly its excellent lateral sensitivity (Reynolds 1997).

The geometric factor becomes relatively large in dipole-dipole surveys. Especially with deeper investigation depths, and following from equation 2.3.2, the voltage potential between the MN electrodes can become very low, and thus lowering the signal to noise ratio or be difficult to measure (Bernard 2003). This is further complicated high ground electrode resistance, resulting in intensity of the current becomes weaker.

High ground electrode resistance was certainly a major problem for the CC' line, which subsequently resulted in a very noisy data set (figure 3.2.8). For this reason this model should be omitted, however it was included as an example of what large resistivity values between the electrodes does to a dipole-dipole survey. The CC' line resulted in about 1/8 of the report points in the pseudosection to have negative values. These are interesting phenomena, but regarded as measurement error and thus filtered out.

The DD' line required very little filtering, and is an example on a more successful measurement than the CC' line. The DD' report point distribution (figure 3.2.9) indicates a more uniform apparent resistivity distribution or much less noise. The wide distributions of values in the top layer are the effect from a dryer hill in the middle of the survey line.

The BB' line had a slightly different setup, with 3 meter spacing between each electrode. This configuration does not penetrate as far down as the other, but it does have a greater resolution than the others (Bernard 2003). There are no other significant differences in this model from

the others. This was the only one oblique to West South direction, and it may indicate a dipping up layer southwards. The resistivity values are in the same range as for the other models.

4.2.6 The Upper layer

All models show a heterogeneous top layer. Large blocks with high resistivity values are intermixed with layers with lower resistivity values. The blocks with high (800-1000 ohmm) values may have numerous explanations. They might be ice rafted debris or drop stones which certainly will have higher resistivity values than the surrounding material. According to Lønne (1993) Ice rafted debris can be expected in deposits like these. Numerous of large boulders up to 5-6 meters in diameter can be seen scattered throughout the deposit, and as Sørensen (1981) further mentioned these boulders seems to be more frequently at the ice proximal side. These large boulders will have higher resistivity values than the surrounding areas, but it should be emphasized that in resistivity models there will never be an abrupt change in values (Hauck and Kneisel 2008), instead a mild transition from high to low will be observed. This is to some extent attenuated by the robust inversion done here, but nevertheless the physical size of these pockets should be treated as relative and not absolute.

The static water table is 0.5 to 1 meter under the surface. The models do not depict this very well, except the DD' line which has a dry hill with high resistivity values attributed to it.

They can also be attributed to gravel lenses, as these encountered during installation of the observation wells by NGI in the summer of 2010 (Kristjansson 2010). This might give a more plausible explanation than the drop stones since the values are not in the bedrock range (Palacky 1987; Solberg *et al*. 2011), however any secondary porosity in the drop stones will lower the electrical conductivity (Reynolds 1997).

The lower resistivity values in the upper part of the model can be attributed to clay lenses, or presence of a lower resistivity material such as graphite or silt. These clay lenses might be the result of cohesive debris flow, which Lønne (1993) claims can be found in several of the A and D units in the conceptual model (figure 2.1.3). One good example of this might be the lower resistivity band in the 4.2.2 model, which seems to extend throughout the whole section. There is evidence of this band in the other models as well, but they are not as

pronounced as the one in the 4.2.2 model. This can be explained by the better resolution of this model.

Another explanation of the heterogeneity might be measurement errors or inversion errors. A measurement error might be the influence of a faulty electrode. This will create a clearly visible higher or lower resistivity values following this electrode downwards will be easy to recognize (Bernard 2003). The only measurement which had a major influence of faulty electrodes was the CC' line, this effect was filtered down.

4.2.7 The interface between the two layers

The interface of the two distinct lithologic layers is for the southwards models at around 13-14 meters. There is however, on the northernmost model (4.2.4) a different depth to the interface, at about - 21 meters. Since the topography was estimated from maps, and not more accurate instruments; and from the models that the insertion of topography had such an effect, this should also be viewed as an estimate. This difference in depth may also be attributed to the difference in terrain height between the different measurement lines.

The model in 4.2.2, the only oblique to west south measurement direction, indicates the interface is slightly dipping upwards when moving north to south. This combined with the deeper depth in the northernmost measurement indicates that the interface is dipping up, however this is only an observation of one line and should be investigated further.

For the west east distribution the interface between the two layers seems to be horizontal.

4.2.8 The lower layer

This deposit is surrounded by salt water on three sides. In settings like these the salt water can be expected to lie under a lens of freshwater, as a described by the Ghyben-Hertzberg relationship (Bear 1979). Salt water values are indicated a range from 0.1 to 1 ohmm (Palacky 1987, Solberg *et al*. 2011). The values from around 2-5 ohmmeter correspond well to salinity values measured by Magnusson and Molvær (1997) and may serve as a good explanation for the change in electrical conductivity if this saline water penetrates the lower parts of the deposit. Salt water intrusion is not uncommon in coastal aquifers since the less dense freshwater tend to overlie the denser saltwater (Schwartz and Zhang 2003). There should be a zone of diffusion between these though; this zone is not very pronounced on the models. This

zone should have a slight increase in electrical conductivity downwards. This might be diminished by the robust inversion performed on the models, and cannot be discarded as a possible explanation for the two layered model based on resistivity measurements alone.

The resistivity values in the lower layers reaches from approximately 2 to 50 ohmmeters, apart from the CC' (figure 4.2.3) model which should not be lent any credibility.

These values correspond well to non-leached marine clay values (Palacky 1987, Solberg *et al.* 2011), but may have another explanation as well. Cuttings from drilling in the summer of 2010 did not show any evidence of a pure clay layer in that depth.

A possible interpretation of the surveys may be that the lithology changes from being grain supported to having a more clay / silt supported matrix structure. Owing to higher electrical conductivity values than the surrounding rocks, this presence of clay and silt will lower the resistivity readings from that depth (Reynolds 1997).

This hypothesis corresponds rather well to the lithologic log (fig. 4.1.1) and grain size distribution charts (figs 4.1.2 and 4.1.3). The models indicate that the interface is located higher up; however this may be a result of the inversion routine or the subsurface lithology (Hauck and Kneisel 2008).

4.2.9 Noise and geoelectrics assumptions

As indicated in figure 2.4.3 noise can affect the electrical readings, Telluric currents can distort the readings. Perhaps the largest influence, at least for some of these readings is the industrial noise at this site. Overhead power masts are in the vicinity, as well as buried cables driving electrical shakers and other mining equipment.

One of the major assumptions in geoelectrics is that the changes in subsurface lithology are fairly horizontal, any deviation from this will result in anomalous features in the inversion routine (Reynolds 1997). However, the horizontal layering seems to be fulfilled here, at least in the West East direction.

4.2.10 Conclusion of the Electrical surveys

All produced models represent a two layered resistivity structure of the subsurface. This was complemented with depth data from the samples collected in the 1980s indicates an interface to a higher conductive saline water or clay / silt rich layer at between 10-30 meters. This layer will be treated as a confining layer, based on these surveys and the work by Sørensen (1981), and establish the basement of the unconfined aquifer for the further models.

The degree of confining layer is questionable; this might be a leaky aquifer. This cannot be concluded on the base of these resistivity surveys. The shallow aquifer will be treated as an non-leaky unconfined aquifer for modeling purposes. This is an assumption for the further work, even though in nature absolute unconfined or confined aquifers are rare (Schwartz and Zhang 2003).

To tie this conclusion to the idealized allostratigraphic model of an ice-contact fan by Lønne (1993) (figure 2.1.3), one possible explanation for the two layer model can be that a subunit 3 is directly underlain by a subunit 4, e.g. B_3 is deposited on top of A_4. It should be again noted that in the areas of measurement there has been heavy excavation so the location is deep inside the original deposit. The theory that the lower conductive layer dips up southwards is not easily explained by this model. However, there is evidence that the glacier's front oscillated (Sørensen 1981, Lønne 1993), and this might complicate the stratigraphy of the deposit, especially the deposition of the B-units.

4.2.11 Establishing the aquifer basement

Based on the grain sizes and the ERT surveys it is unclear at which depth to establish the aquifer basement. The ERT indicates a uniform basement whereas the depth differs from the confining layer found in the grain sizes. However the ERT are models and the grain size is perhaps a better representative for the actual lithology, at least when it comes to the depth estimates.

For this thesis the aquifer will be assumed to be 20 meter based on the grain size samples and the distribution of this layer is confirmed by the ERT models. However, for the pumping test different depths to aquifer basement will be modeled.

4.3 The tidal method results

4.3.1 Estimates of the aquifer's diffusivity from the FFT.

The results from the water level and tidal observations and the FFT gave the aquifer diffusivity estimates presented in table 4.3.1

Table 4.3.1 Results from Tidal Forcing method

Tidal constituent	Efficiency diffusivity [m^2/day]	Lag based diffusivity [m^2/day]
M_{Sf}	4466.00	248986.19
M_2	11051.47	425.61

There is a large difference between the lag and the efficiency based calculations.

The two lag based estimates produced very unrealistic results, and this is in accordance with other studies done with this method (Jha *et al*. 2008) and Merrit (2004). The lag results will be discarded as possible values for this aquifer.

However, the efficiency based results does not deviate so strongly from each other and will be investigated further. According to table 2.1.1 these values fall in the Fine Sand / Coarse Sand range.

4.3.2 Comments and conclusion of the tidal estimates

The analysis based on these observations depends largely of identifying the tidal constituents and their amplitude and their phase. This was done with comparing the amplitude spectra created from tide and well observations.

The results may not be very reliable since the assumption of a confined aquifer is not fulfilled from Ferris (1951). However, the two efficiency based results are not highly unlikely and will be compared to those from the pumping test, although they represent two different areas of the aquifer; the tide method measures to a large extent the marine shore deposits as categorized by Sørensen *et al*. (1990) (figure 2.1.5) whereas the pumping test is done in glaciofluvium.

Numerous errors may influence this data set; however these are dependent on the accuracy of the measurement of the head in the wells, and successfully subtracted from the atmospheric level. It was assumed that the fluctuations of the air pressure and the well level had a ratio of 1:1; this might not be the case, since the air pressure also has an effect on the tidal level which again is in contact with the aquifer.

Jha *et al*. (2008) concluded that the speed of tide propagation is faster than the model-prediction by Ferris (1951). This will result in erroneous estimates of the aquifer parameters with the lag method. Further the conclusion was that the use of time lag method for estimating hydraulic diffusivity should be avoided, it can however; give a crude estimate of the hydraulic parameters.

Further assumptions of the method apart from the confined aquifer, is that the aquifer should be homogeneous, isotropic, semi-infinite (Ferris 1951), none which holds true for this setting.

The geographical setting of the aquifer, it is surrounded by a tidal body on three sides may further complicate the tidal signal as well, this formula is based on a one dimensional transient propagation of a sinusoid signal (Ferris 1951; Todd 1980).

Furthermore, the observation wells placed inland are not perfect. They do show changes in hydraulic head which is in accordance with the tidal fluctuations measured at SVR01, but the well losses may decrease the amplitude generated by tidal fluctuations.

This experiment will then follow the same conclusion as Jha *et al*. (2008); Merritt (2004) that the tidal method for estimating the aquifer's hydraulic diffusivity should be used with caution, and be applied only as a crude indication.

A quicker way to find the aquifer diffusivity from short observation series is to use equation 2.4.1 and use the efficiency based formula in equation 2.4.5.

4.4 Results and discussion from the pumping tests

The application Aqtesolv (Hydrosolve Inc.) was used to fit the analytical solutions to the observed data series. The Theis analytical model is represented with a blue line in the following graphs. This was fitted to the drawdown curve. The aquifer's saturated thickness is not known with certainty, so different depths and anisotropy ratios were applied.

4.4.1 Results from the Theis analytical models

All following figures portray the observed drawdown in the GR08 well as squares and the Theis analytical solution as the blue line.

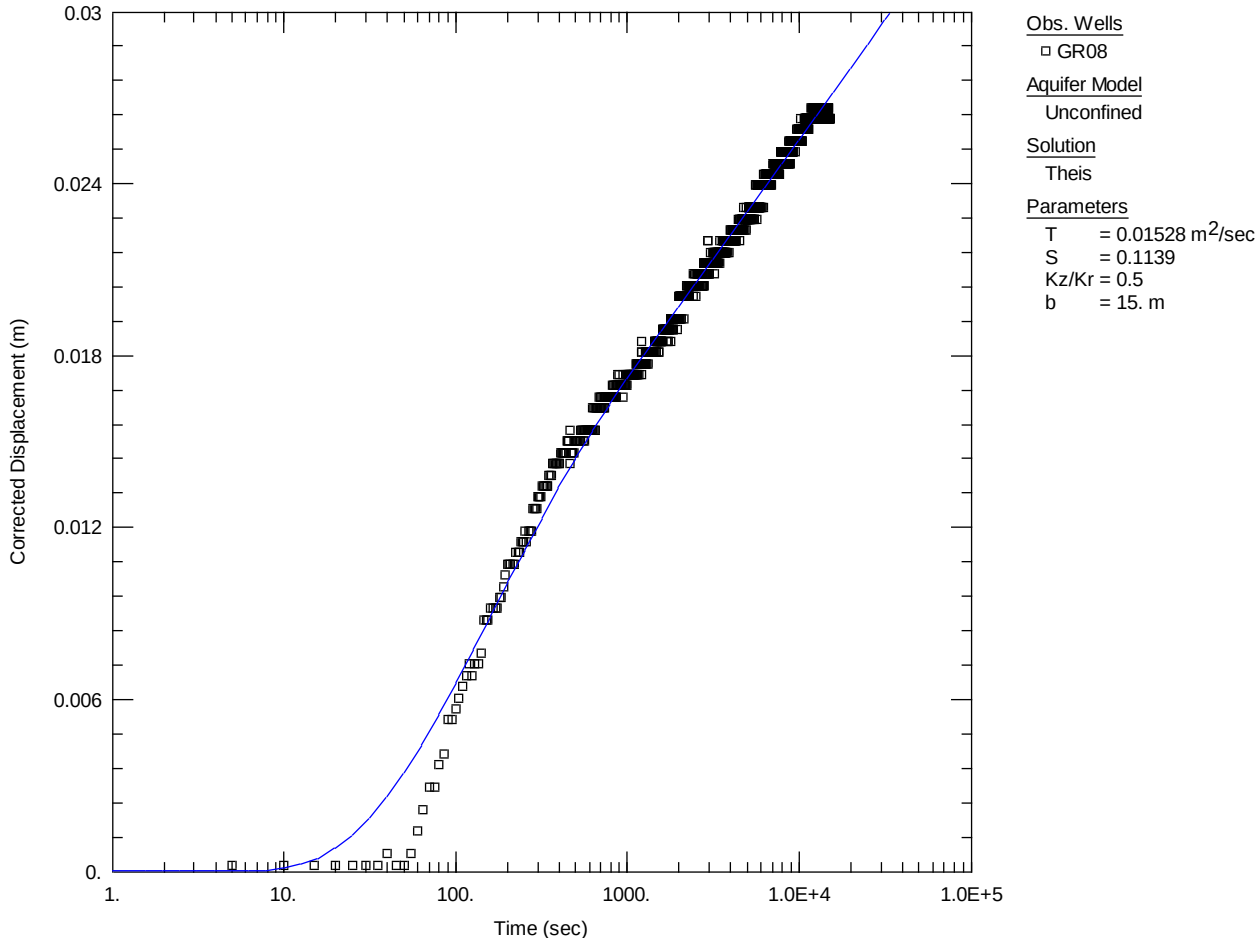

Figure 4.4.1 Analytical results in GR08 15 meters aquifer base anisotropic ratio 0.5

The solution presented in figure 4.4.1 with an anisotropic ratio of 0.5, the resulting transmissivity is 1,528 x 10^{-2} m^2s^{-1} and storativity 0.1139. This gives diffusivity (T/S) of 0.1314 m^2s^{-1}, or converted to 11590.8 m^2d^{-1}.

For an anisotropy ratio of 1, the model gave:

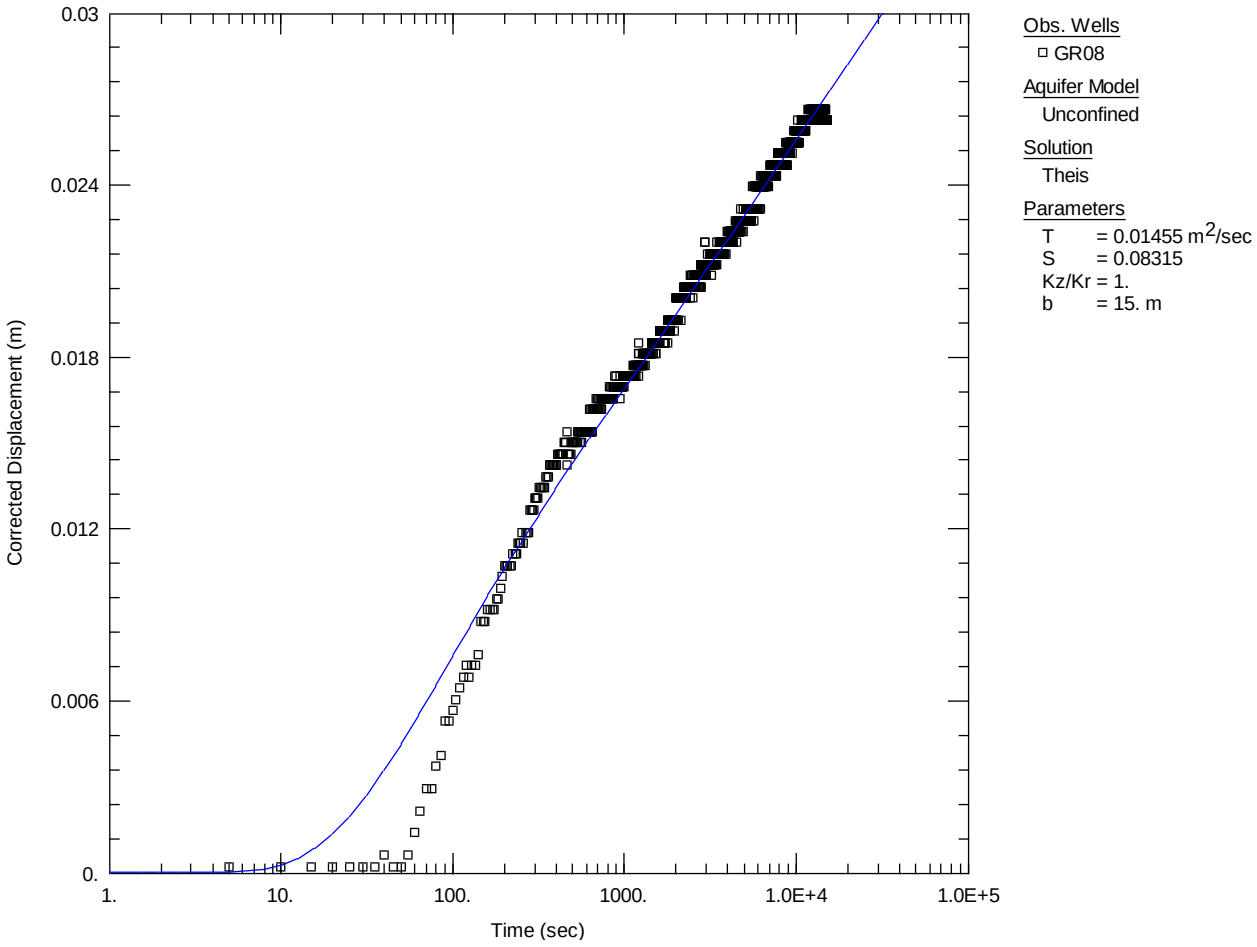

Figure 4.4.2 Analytical results in GR08 15 meters aquifer base anisotropic ratio of 1

The solution in figure 4.4.2 gave with an anisotropic ratio of 0.5; transmissivity is 1,455 x 10^{-2} m^2s^{-1} and storativity 0.08315.

This gives diffusivity (T/S) of 0.1750 m^2s^{-1}, or converted to 15118.7 m^2d^{-1}.

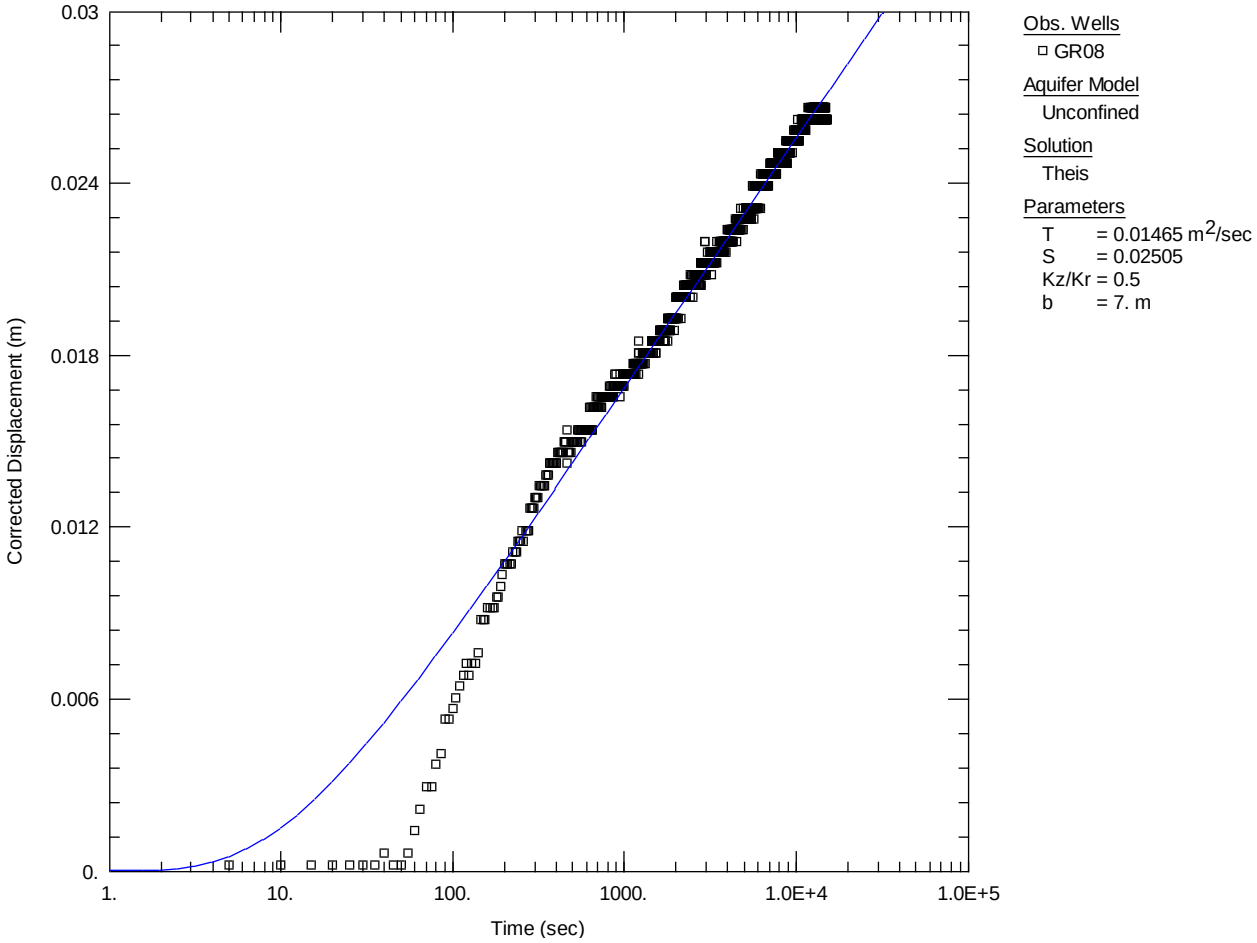

Figure 4.4.3 Analytical model with aquifer base at 7 meters

There were miniscule differences in T/S with the different anisotropic ratios.

This solution in 4.4.3 with an anisotropic ratio of 0.5, gave transmissivity is 1,465 x 10^{-2} m^2s^{-1} and storativity 0.02505.

This yields diffusivity (T/S) of 0.0584 m^2s^{-1}, or converted to 50529 m^2d^{-1}.

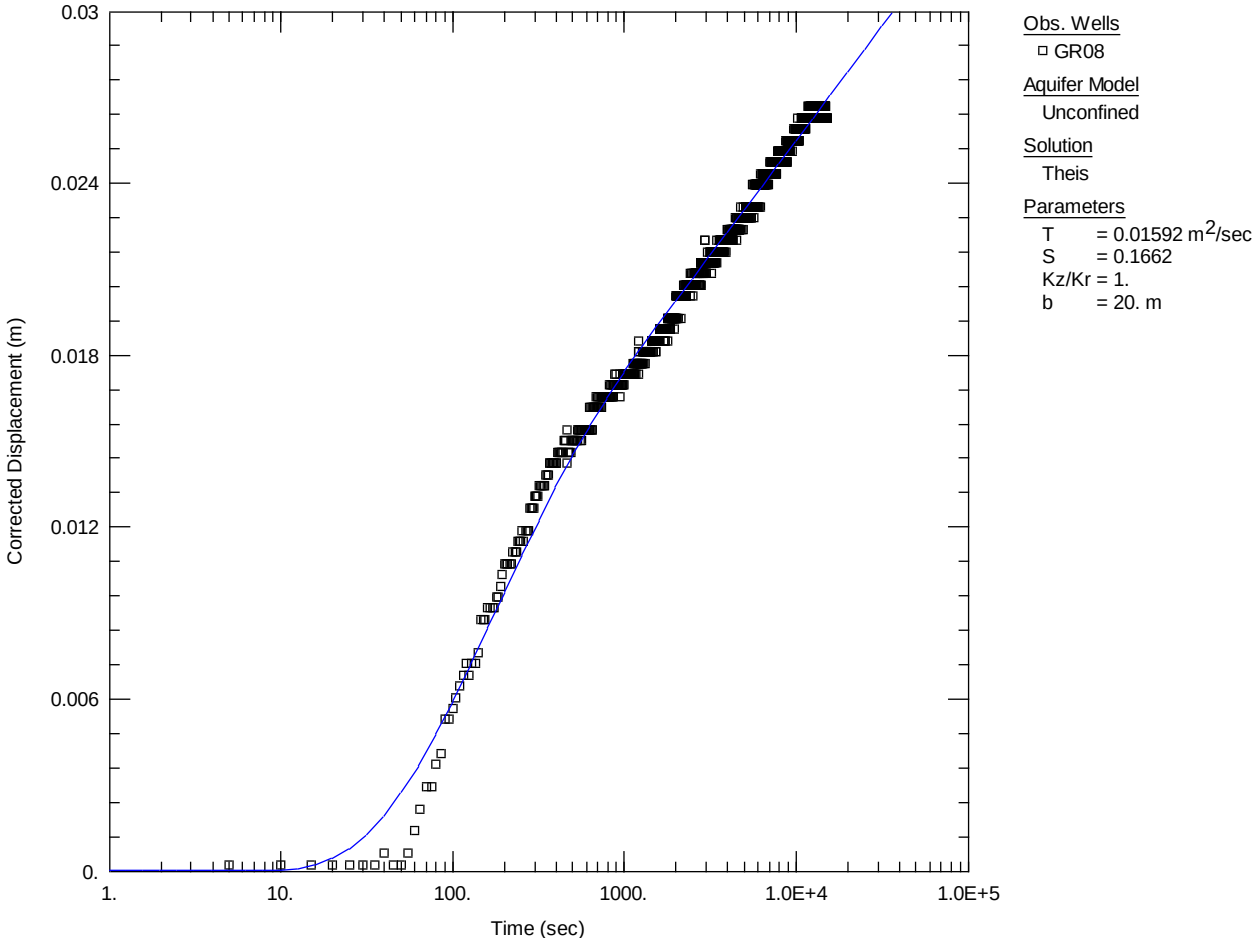

Figure 4.4.4 Analytical results in GR08 with 20 meter base

A 20 meter thick aquifer gave the solution presented in figure 4.4.4 and with an anisotropic ratio of 1 gave transmissivity is 1,592 x 10^{-2} m^2s^{-1} and storativity 0.1662.

This gives diffusivity (T/S) of 0.095 m^2s^{-1}, or converted to 8276.1 m^2d^{-1}.

For the anisotropic ratio of 0.5, the resulting transmissivity is 1.803 x 10^{-2} m^2s^{-1} and storativity 0.2. This gives diffusivity (T/S) of 0.09 m^2s^{-1}, or converted to 7734.8 m^2d^{-1}.

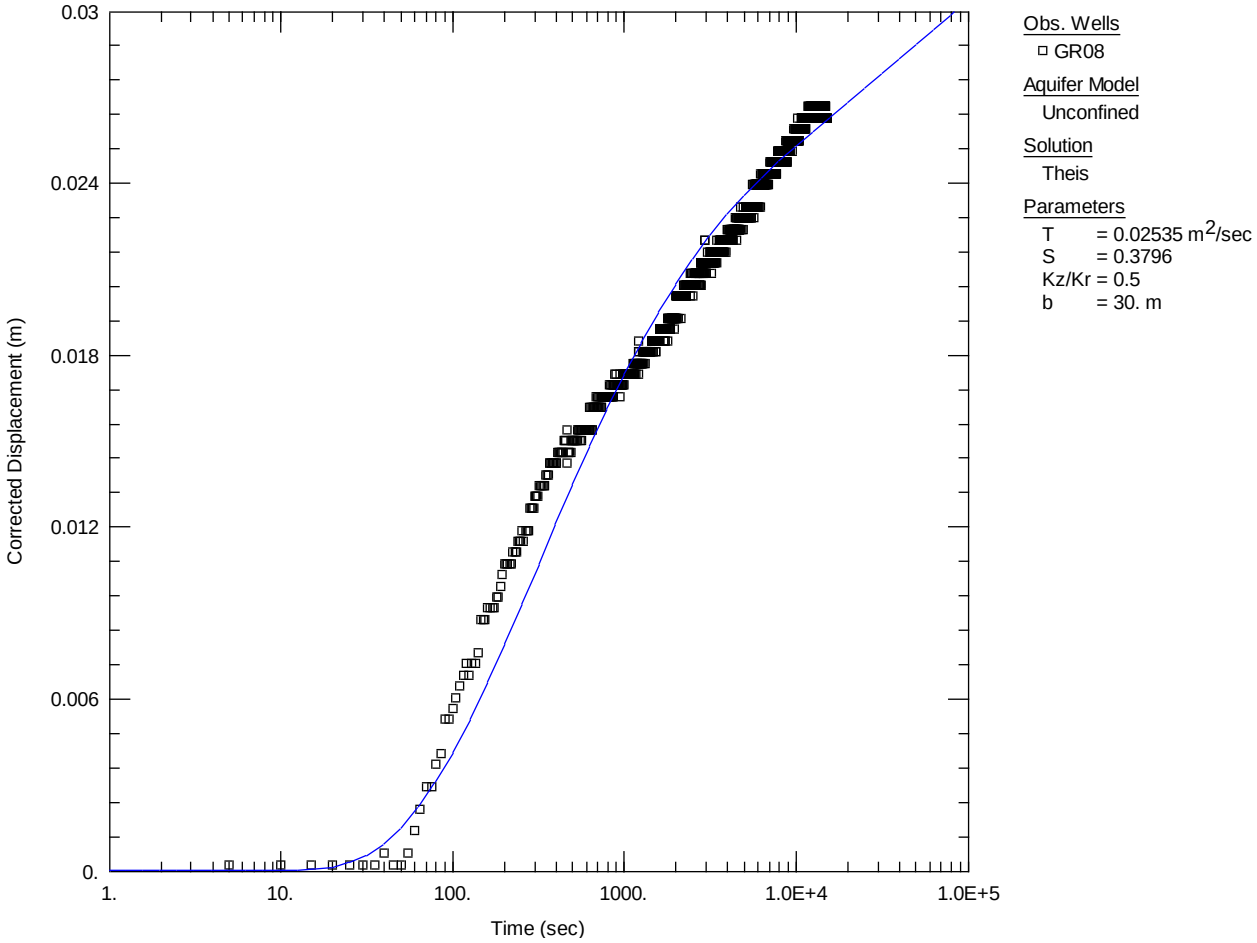

Figure 4.4.5 Analytical results in GR08 with 30 meter base

A 30 meter basement solution in figure 4.4.5 with anisotropy ratio of 0.5, resulted in transmissivity is 2.535 x 10^{-2} m^2s^{-1} and storativity 0.3796.

This gives diffusivity (T/S) of 0.067 m^2s^{-1}, or converted to 5769.9 m^2d^{-1}.

4.4.2 Comments on the pumping test results

The goodness of fit is dependent on where in the data set the Theis curve is fitted. As described in section 3.4 the curve for an unconfined aquifer at early time will fall on a Theis curve. At intermediate time, the delayed gravity drainage will be influential, and thus lower the curve, deviating from the Theis curve. At late time the model should adhere again to the Theis curve, and the storativity will be the same as the specific yield (Kresic 2007). By fitting the Theis curve at early time, the storativity values will be similar to that of a confined aquifer, and will be much lower than they really are in an unconfined aquifer. So, the models are fitted to the late time data.

This problem has been examined by several, and Nwankwor *et al.* (1992) claims that it is usual to fit the Theis curve to early time data, but it should for all practical reasons be fitted to the late time data, after delayed gravity drainage. This is further supported by at early time the water yielded comes mainly from elastic drainage in the soil matrix (Driscoll 1986). Then storativity values will be too low for an unconfined aquifer (Schwartz and Zhang 2003).

Fitting the model to late time data implies that the duration of the pumping test to be rather long, which for this test does not hold true. However the flat trend in the derivative plot (figure 3.4.4) indicates that the gravity response is more or less completed at late time, and subsequently the specific yield can be estimated with more reliable results than at early time.

The estimated aquifer saturated thickness of 20 meters found from the ERT and flush samples correlates well with the 20 meter model in figure 4.4.4. The other models show poorer fits, especially for the 30 meters model. However, the models omitting the 30 meter model show relative good fits at late time data.

4.4.3 Assumptions for the Theis method

A numbered list of the assumptions was listed in section 2.5.4

- The infinite-acting (first) assumption is met. Observations in well BR01 during the test indicated no influence by the drawdown in BR03. There are no visible boundaries adjacent to the pumping test site, e.g. mountains or other impervious boundaries.
- The second assumption that the aquifer is homogeneous is far from being met, judging from the resistivity models and also from the lithologic log presented (figure 4.1.1).

The isotropy assumption is not met either. These assumptions are rarely seen in nature and it would be very difficult to model the true nature of the aquifer.

- The aquifer does not have a uniform thickness as indicated by the electrical resistivity models, but for the area influenced by the pumping test it can be assumed that the aquifer is close to having uniform thickness. This is not true when the water table is lowered around the pumping well. However in this test the cone of depression is small and will subsequently have a miniscule effect on the saturated thickness.
- The pumping well partially penetrates the aquifer, and thus assumption number 4 can be discarded. The fifth assumption is met, being that the aquifer is unconfined. Flow is transient, this can be seen from the observation graphs that the water table fluctuates as a result to tidal forcing; thus assumption number 6 is met.
- The seventh assumption, that water is released instantaneously from storage with a decline of hydraulic head is not met either. This assumption stems from that this solution is made for the use of confined aquifers. For unconfined ones it takes some time before the water is drained as a response to a change in head (Driscoll 1986). Further testing needs to be performed to ascertain this time and thus the delayed gravity response is not taken into account. Another analytical solution, such as Moench (1997) can take this into account when fitting the curve.
- The eighth assumption is not met either, the diameter of the PVC casing is 10 cm, however the outer casing is larger so it takes time before the existing water is abstracted from the well. This can be seen that it takes almost a minute before any observable drawdown in the GR08 well after pumping has commenced. This is further complicated by the well was drilled with mud. This contributes to a positive skin effect.
- The ninth assumption is not common to be met for unconfined aquifers, and this is not the case for this aquifer either. However, the drawdown plots does not indicate a substantial delayed gravity yield (compare figure 2.5.3b to 3.4.3), but it cannot be said that this assumption is met.
- The 10^{th} condition stems from the Dupuit assumption for unconfined aquifer flow and further relates to the unconfined aquifer correction (formula 2.5.5) for drawdown in unconfined aquifers. This is difficult to give an estimate of, and cannot be answered if this is satisfied or not. The same can be said for assumption 11, not possible to

ascertain if the flow is horizontal and uniform. However, there are no indications that this is not the case.

- For the last assumption (12) the depression was relatively small. Maximum drawdown in GR08 was 0.25 meters (figure 3.4.1)

4.4.4 Transmissivity results

The Transmissivity results from the Theis analytical models are all in the area of 10^{-2} m^2s^{-1}. For an aquifer with saturated thickness of 20 meters this gives an average hydraulic conductivity for $10^{-3}ms^{-1}$. According to Bear (1979) this is between good to poor aquifer permeability and is subsequently classified as sand or sand/gravel to VF sand to silt. This corresponds well with the lithology described in the lithologic log (figure 4.1.1).

In general higher transmissivity values results in a lower drawdown effect at a pumped well (Kresic 2007), and subsequently the amount of water abstracted from the well will have to be higher for successful measurement of drawdown in nearby observation wells.

4.4.5 Storativity results

The specific yield values for unconfined aquifers varies generally between 0.05 and 0.3, but higher and lower values may be seen in finer grained or less uniform material (Kresic 2007). However, a more reliable way to find out more about this parameter is to do laboratory testing on a sample which contains the main characteristics of the aquifer (Schwartz and Zhang 2003). For this aquifer this has not been done, but still according to Nwankwor *et al*. (1992), a pumping test estimate should give a good approximation. The value is dependent on the aquifer properties such as the anisotropy ratio and the aquifer thickness. This was the case here as well and the results from the analytical models ranged from 0.37 with 30 meter saturated thickness to 0.02 for the 7 meter saturated thickness. The 0.37 is a very large value for this type of aquifer and 0.02 is very low. According to Kresic (2007) the values for medium sand and gravel (lithology according BH1, figure 4.1.1) ranges from 0.1 to 0.2 so it is plausible that the storativity values fall in this range, this is in accordance with the 20 meter depth analytical model (figure 4.4.4).

4.4.6 Comments on errors on the pumping tests and analytical models

First and foremost many of the assumptions for this analytical solution listed in section 2.5.4 were not met. However, the drawdown resembles curves for confined aquifers (figure 2.5.3a); this can justify the use of the Theis analytical model (Krusemann and de Ridder 1992). According to the diagnostic plots, the biggest influence from the diagnostic plots is the skin effect. Theis (1935) does not take into account this, and another analytical solution should be used to see if there is any major change in the parameters.

Another limiting factor of this test is that it only measures between the pumping well and the observation well. For this case this was 4 meters, and the results cannot be said to be representative for the whole deposit. This is also true for the vertical distribution, and from the lithologic log, the lithology changes with depth and accordingly would the parameters that govern groundwater flow.

4.4.7 Comparison between tidal forcing results, pumping test results and hydraulic conductivity estimates from the samples

For this comparison the 20 meter saturated thickness was used based on the resistivity models and the lithologic log. The results are presented in figure 4.4.1. K denotes the hydraulic conductivity.

Table 4.4.1 Pumping test results

Saturated thickness(m)	Anisotropy ratio	Transmissivity (m2/s)	Storativity	Estimated K (m/s)
20	1	1.59E-02	0.166	7.96E-04
20	0.5	1.80E-02	0.2	9.00E-04

The results from the tidal forcing method with a saturated thickness of 20 meters gave the results presented in table 4.4.2.

Table 4.4.2 Tidal Forcing Efficiency based estimates

Saturated thickness(m)	Efficiency based diffusivity (m2/d)	Transmissivity (m2/s)	Estimated Storativity	Estimated K (m/s)
20	4466	8.27E-03	0.16	4.14E-04
20	4466	1.03E-02	0.2	5.17E-04
20	11051	2.05E-02	0.16	1.02E-03
20	11051	2.56E-02	0.2	1.28E-03

Based on the 20 meter saturated aquifer thickness the tidal forcing method with a storage coefficient values from the pumping tests this gave hydraulic conductivity estimates in the range of 10^{-3} to 10^{-4} ms^{-1}. The end result is dependent on which tidal constituent which is used. The longer period of the M_{sf} gave lower hydraulic conductivities than the shorter period of the M_2 constituent; this relationship can be seen in equation 2.4.5. This correlates to gravel to fine sand lithology in table 2.2.1.

The pumping test analyzed for the GR08 well by Kristjansson (2010) gave a transmissivity value of 1.3 x 10^{-2} ms^{-1}. BRGM (2010) estimated a transmissivity value of 1.64 x 10^{-2} $ms^{-1.}$

The hydraulic conductivity estimates from the grain size distribution charts presented in section 4.1 resulted in the upper 7 meters (samples # 1 and 5) hydraulic conductivity values in the lower end of 10^{-4} ms^{-1}.

The values from the pumping tests resulted in hydraulic conductivity values in the upper 10^{-4} ms^{-1}. These values correspond to the gravel to fine sand range according to table 2.2.1. This corresponds well to Lønne (1993) with the diamictic material deposited by a glacier.

5 CONCLUSION AND RECCOMENDATIONS

This study aimed to categorize the hydrogeology of the unconfined aquifer at the Svelvik ridge in southeastern Norway. For this categorization several factors are needed; these are the saturated thickness, transmissivity and storativity. For this thesis the saturated thickness was found by comparing two methods.

The first method was based on flush samples from a drilling operation. The results indicated a retarding layer at circa 20 meters. This depth was compared to resistivity models from dipole-dipole surveys. The presence of an interface was confirmed with the resistivity models; however the depth to this interface was not confirmed.

The hydraulic conductivity estimates from the two methods applied resulted in values in the range of 10^{-3} to 10^{-4} ms^{-1}. These correlates to a gravelly to sand lithology which is in accordance with models of ice contact submarine fans and the samples collected from drilling operations.

The lag based estimates from the tidal forcing method gave unreliable results, however the efficiency based estimated gave results similar to that of the pumping tests.

For more information about the characteristics of the retarding layer an Induced Polarization survey should be done. If this confirms the presence of a clay / silt layer, an RCPTU survey should be done to accurately pinpoint the depth to the interface. This can be substituted by a well logging operation with resistivity equipment. This can be further investigated with ground penetrating radar and seismic surveys. A more detailed vertical description of the aquifer will return a more accurate estimation of the hydrogeological parameters.

For a more detailed tidal test the duration of observation should be longer. This would identify more tidal constituents and give more estimates of the diffusivity. Further, additional wells could be installed closer to the shore than 120 meters, to observe the rates of attenuation of the signals. It would be interesting to see how the deposit is influenced by the tides on the northern side and at the western side.

The pumping test should be of a longer duration and use a more powerful pump to lower the drawdown in the formation. The pumping well should be stimulated with pulsing technology to diminish skin effects.

A laboratory analysis on representative samples from the aquifer should be done to ascertain the storage coefficient and the anisotropy ratio in greater detail. More accurate values for these parameters will give better estimates for the transmissivity and hydraulic conductivity.

Literature cited

Barker, R.D. (1989) Depth of investigation of collinear symmetrical four-electrode arrays. *Geophysics*. 54:1031-1037.

Bear, J. (1979) *Hydraulics of Groundwater*, McGraw-Hill, New York, USA 569p.

Bernard, J. (2003) J. Bernard, Short Note on the Depth of Investigation of Electrical Methods, Iris Instruments, Orleans, France.

Bjerkli, K and Olsen, H.A. (1984) Refleksjonsseismiske malinger i Drammensfjorden. Norges Geologiske Undersøkelse, Rapport 84.12.

BRGM (2010) Permeability tests of the shallow well (6 m) Unpublished data.

Driscoll, F.G. (1986) Groundwater and Wells. Johnson Filtration Systems Inc., St. Paul, MN

Defant, F. (1961) Local winds. Compendium of Meteorology, T. F. Malone, Ed., American Meteorological Society. pp. 655–672

Domenico, P. A. and Schwartz, F.W. (1998) Physical and chemical hydrogeology (Second editions), John Wiley & Sons, New York, USA.

Erskine, A.D. (1991) The effect of tidal fluctuations on a coastal aquifer in the UK. Ground Water 29, 556–562

Ferris, J.G. (1951) Cyclic fluctuations of a water level as a basis for determining aquifer transmissivity. International Association of Scientific Hydrology Publication 33, 148–155.

Gustafson, G., Andersson, A-C and Andersson, O. (1984) Brunnar. Undersøking-Dimensionering-Borrning-Drift. Byggforskningsrådet, Rapport 42.

Hazen, A. (1893) Some physical properties of sands and gravels with special reference to their use in filtration. 24th Annual Report, Massachusetts State Board of Health, Boston.

Hauck C, Kneisel C. (2008) Applied Geophysics in Periglacial Environments. Cambridge University Press: Cambridge; 240 pp

Jarosz, E. (1997) Tidal dynamics in the Bab el Mandab Strait. Doctor of Philosopy thesis, Department of Oceanography and Coastal Sciences, Louisiana State University, USA.

Jha MK, Namgial D, Kamii Y, Pfeiffer S. (2008) Hydraulic parameters of coastal aquifer systems by direct methods and an extended tide–aquifer interaction technique. Water Resource Management. DOI:10.1007/s11269-008-9259-3

Kristjansson, Bjarni, R. (2010) Hydrogeological investigation of the shallow aquifer at Svelvik ridge, Drammensfjorden. Norges Geotekniske Institiutt, Oslo.

Kresic N. (2007) Hydrogeology and Groundwater Modeling, Second Edition. CRC Press/Taylor & Francis, Boca Raton, New York, London, 807 p.

Krusemann, G.P. and DeRidder, N.A. (1992) Analysis and Evaluation of Pumping Test Data (2nd ed.), Publication 47, Intern. Inst. for Land Reclamation and Improvement, Wageningen, The Netherlands, 370p.

Lønne, I. (1993) Sedimentary facies and depositional architecture of ice-contact glaciomarine systems. Dr. Scient Thesis, Department of Soils and Water Sciences, Agricultural University of Norway. Ås.

Moench, A.F.(1997) Flow to a well of finite diameter in a homogeneous, anisotropic water-table aquifer, Water Resources Research, vol. 33, no. 6, pp. 1397-1407.

Norges Geologiske Undersøkelse (2011) Available at : http://www.ngu.no/no/hm/Georessurser/Naturstein/Viktige-natursteinsforekomster/Drammensgranitten/ Visited May 27, 2011

Nwankwor, G. I., R. W. Gillham, G. van der Kamp and F.F. Akindunni (1992) Unsaturated and saturated flow in response to pumping of an unconfined aquifer: Field evidence of delayed drainage. Ground Water. V. 30, no. 5 pp. 690-700-.

Magnusson, J. and J. Molvær (1997) Transfjo. Hydrophysical observations in the Frierfjord, the Drammensfjord and the Iddefjord July-December 1997. Data report. Report, NIVA-Oslo No. 3951-97, 40 p.

Merritt, Michael, L. (2004) Estimating Hydraulic Properties of the Floridian Aquifer System by Analysis of Earth-Tide, Ocean-Tide, and Barometric Effects, Collier and Hendry Counties, Florida: U.S. Geological Survey Water-Resources Investigations Report 03-4267, 70 p.

Palacky, G.J. (1987) Resistivity characteristics of geological targets. I: Nabighian, M.N.: Electromagnetic methods in applied geophysics. Society of Exploration. Geophysics., Tulsa

Renard, P. D., Damian, G., Mejias, M. (2008) Understanding diagnostic plots for well-test interpretation., Hydrogeology Journal vol 17, No 3, DOI : 10.1007/s10040-008-0392-0

Reynolds, J.M. (1997) An introduction to applied and environmental geophysics. John Wiley and Sons, Inc., England

Schwartz F.W and Zhang H. (2003) Fundamentals of Groundwater. New York: John Wiley & Sons, Inc., p.30-360.

Smith, A.J., Hick, W.P. (2001) Hydrogeology and Aquifer Tidal Propagation in Cockburn Sound, Western Australia. CSIRO Technical Report 6/01.

Solberg Inger-Lise, Louise Hansen, Jan Steinar Rønning & Einar Dalsegg (2011) : Veileder for bruk av resistivitetsmålinger i potensielle kvikkleireområder. Versjon 1. Norges geologiske undersøkelse. Rapport 2010.048

Sørensen, R., Lie, K.T. and Nybakken, S.E. (1990) DRØBAK 1814 II, kvartærgeologisk kart – M 1 :50 000. Norges geologiske undersøkelse.

Sørensen, R. (1981) Foreløpig beskrivelse til kvartærgeologisk kart SVELVIK – CL 083, M1:10 000 Norges geologiske undersøkelse, Rapport 1807/7 -1981

Theis, C.V. (1935) The relation between the lowering of the piezometric surface and the rate and duration of discharge of a well using groundwater storage, Am. Geophys. Union Trans., vol. 16, pp. 519-524.

Todd, K.T. (1980) Groundwater Hydrology (Second edition). University of California, Berkeley. J. Wiley & Sons.

Weisstein, Eric, W. (2002) CRC Concise Encyclopedia of Mathematics (Second Edition) CRC Press, Boca Raton, FL, USA

Acknowledgments

The author wants to thank:

Fridtjov Ruden for tremendous inspiration and motivation. Thank you again for everything you have taught me about hydrogeology and resistivity methods.

Per Aagaard for supervision.

Eyvind Aker at NGI for reading trough and for useful comments and for getting me started with the Fourier Transform.

Kim Rudolph-Lund for teaching me a lot about hydrogeology.

Lena Evensen, for motivation and help with the resistivity measurements.

Dodo Bartucz for much appreciated help with the resistivity measurements.

A very special thanks to my mother and father for always being there with great understanding and support.